2011-01-01

Automated Detection Of Dust Clouds, Sources, And Direction From NOAA-AVHRR Satellite Imagery

Mohammed Qassim Alkhatib
University of Texas at El Paso, mqalkhatib@miners.utep.edu

AUTOMATED DETECTION OF DUST CLOUDS, SOURCES, AND DIRECTION FROM NOAA-AVHRR SATELLITE IMAGERY

Mohammed Qassim Alkhatib

Department of Electrical and Computer Engineering

APPROVED:

Sergio D. Cabrera, Ph.D., Chair

Bryan Usevitch, Ph.D.

Thomas E. Gill, Ph.D.

Benjamin C. Flores, Ph.D.
Acting Dean of the Graduate School

AUTOMATED DETECTION OF DUST CLOUDS, SOURCES, AND DIRECTION FROM NOAA-AVHRR SATELLITE IMAGERY

By

MOHAMMED QASSIM ALKHATIB, B.S.E.E.

THESIS

Presented to the Faculty of the Graduate School of

The University of Texas at El Paso

in Partial Fulfillment

of the Requirements

for the Degree of

MASTER OF SCIENCE

Department of Electrical and Computer Engineering

THE UNIVERSITY OF TEXAS AT EL PASO

December 2011

ACKNOWLEDGMENTS

I would like to take this opportunity to express my sincere thanks to Dr. Sergio Cabrera for his guidance and support, which without him this would not have been possible, I'm also very thankful to him for recommending me to receive the Texas Instruments Foundation (TIF) Scholarship which provided me with financial support to help me pursue this degree.

I would also like to sincerely acknowledge and thank Dr. Bryan Usevitch for his assistance in serving in my committee.

Also I appreciate and thank Dr. Thomas Gill, from the Department of Geosciences, for his advice and for serving in my committee.

ABSTRACT

This research is mainly focused on automatically locating dust sources and estimating their transport direction in NOAA-AVHRR images. Applications of AVHRR images may include agricultural assessment, producing maps of large area, and to retrieve various geophysical parameters. The AVHRR simultaneously records five bands of data, in our research, we focused on bands four and five since these wavelengths highlight the absorption and subsequent emission of thermal radiation by the silicate particles in the dust storms.

In this research, we propose a new method to detect dust clouds on satellite images. The approach we propose involves the use of an image segmentation technique known as region growing. This method starts with a set of seed points obtained from a band math image, which is known to be a good indicator of dust clouds due to physical reasons, the result will be a binary image that represents the improved dust cloud region estimate.

We also propose a method to locate dust sources automatically in satellite images. Previous methods were mainly based on the user manually selecting the source points in the satellite image. The method developed here uses corner detection on the boundary of the dust cloud region.

Also, we propose a new technique for finding the direction of the dust transport in the dust cloud region using individual bands from the NOAA-AVHRR imagery. Multi-resolution filters and state-of-the-art directional filters, based on the Contourlet transform, are used to help us determine the direction with more precision and consistency among the relevant subimages than in previous approach.

Before applying the directional filtering to the candidate region of the multispectral image, a preprocessing step involves passing the image through a nonsubsampled pyramidal transform to apply selective amplification of high frequency information. This preprocessing step enhances the directional streaks before the directional filtering used. For AVHRR images, our methodology involves applying directional filtering on bands 4 or 5. Directional filtering is applied to blocks of the image targeting a decision among 8 or 16 different angles. From the filter outputs, energy measurements are computed to find the prominent direction of the dust storm in each block. The presence of consistent prominent directions in the texture of the blocks that constitute region of the dust storm can be used as a verification of its presence.

TABLE OF CONTENTS

CHAPTER 1

INTRODUCTION

1.1 Multispectral Images and Satellite Imagery

Remote sensing is the technology of getting information for an object without being in actual contact with it. This includes sensing, recording, processing and analyzing that information [1]. Multispectral images are one type of information that can be acquired using satellites. They have opened up new possibilities for monitoring atmospheric events such as dust storms that produce environmental risks. Other applications of multispectral images include change detection, target detection, and classification. Figure 1.1 illustrates a typical remote sensing system.

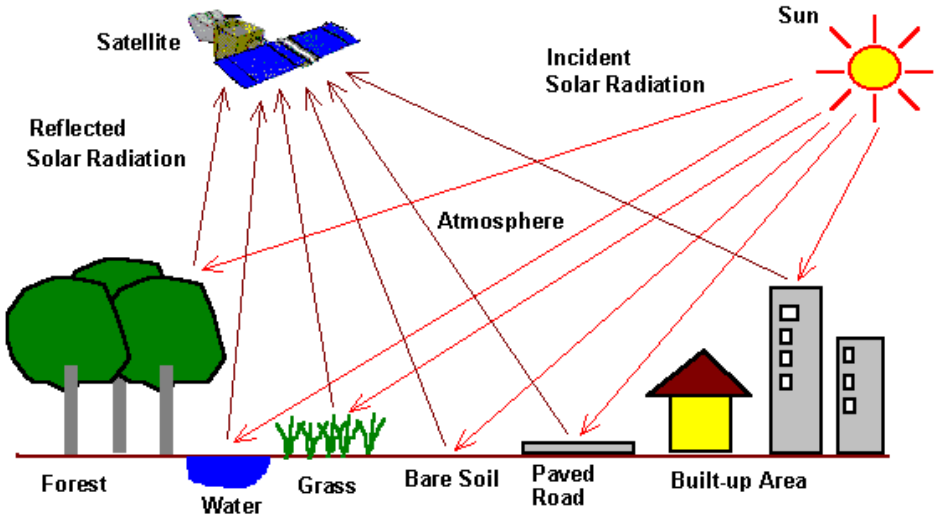

Figure 1.1: overview of Remote sensing system. [18]

Multispectral images have this name from the fact that they separately capture energy in more than one spectral interval of the electromagnetic spectrum. Each image is referred as a band. Satellite imagery produces multispectral images of the earth; each image corresponds to the same

physical area and scale, but at different spectral bands, Figure 1.2 shows the layout of the electromagnetic spectrum.

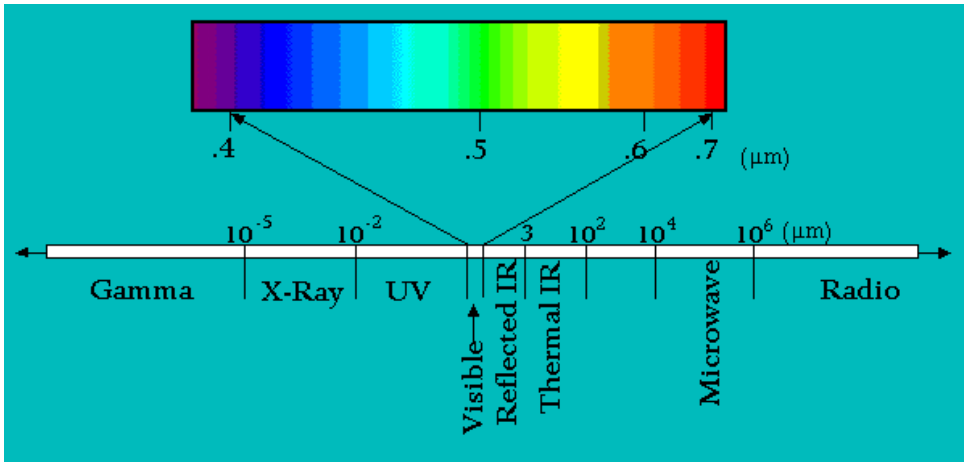

Figure 1.2: Layout of Electromagnetic spectrum [19]

Each band image (channel) that is captured using the satellite carries certain amount of information. These images contain spatial, spectral, and temporal information about that specific earth surface patch. The finite energy that arise from the earth surface is then spatially divided into pixels, a pixel is the smallest single component in a digital image, each pixel is associated with a number called the digital number or brightness value. For satellite images, that number displays the average radiance of a relatively small area within a scene, and it ranges from 0 to 255 in 8-bit bit per pixel image.

Remote sensing data obtained from sensors like the Advanced Very High Resolution Radiometer (AVHRR) aboard a National Oceanic and Atmospheric Administration (NOAA) satellite are used to monitor dust events that occur in the atmosphere. Other sensors like the Geostationary Operational Environmental Satellite (GOES) and the Moderate Resolution Imaging Spectroradiometer (MODIS) are also used to monitor dust events. AVHRR and GOES have 5 spectral bands with a wavelength range from 0.5μm to 12.5μm. MODIS has thirty six spectral

bands ranging in wavelength from 0.405μm to 14.385μm. Among those sensors, GOES is the one that has the least spatial resolution, which is why AVHRR and MODIS are of particular interest. The spatial and temporal resolutions for each sensor are provided in the next table.

Table 1.1: Overview of sensor spatial and temporal resolutions

Sensor	Number of Bands	Spatial Resolution	Coverage
NOAA-AVHRR	5	1 km each	Daily
MODIS	36	Ch1-2 – 250 m Ch3-8 – 500 m Ch9-36 – 1 km	1 to 2 days
GOES	5	Ch1 – 1 km Ch2,4,5 – 4 km Ch3 – 8 km	15 minutes to 3 hours

1.2 Dust Storm Detection and Direction Estimation

Dust Storms are serious causes for several physical, environmental and economic hazards. Air pollution from dust storms is a significant health hazard for people with respiratory diseases and can adversely impact urban areas. There is a direct link between exposure to high-levels of air-borne particle concentrations and the increase in mortality rate from cardio-vascular, respiratory illness and lung cancer. Timely warnings of dust storms must be initiated in populated regions for health concerns and traffic control [3]. Although several traditional methods for detecting dust storms exist, satellite images have difficulties in consistently detecting and distinguishing the dust storm features [2].

In one of the proposed techniques described here, multi-resolution filtering is applied to the dust cloud region to enhance image features, this step was necessary to enhance the performance of the directional filter, which is applied on Band 4 and Band 5 to estimate the direction of motion of the transport from the dust storm. Band 4 (10.3µm - 11.3µm) and Band 5 (11.5µm - 12.50µm) are of interest since they highlight the absorption and subsequent emission of thermal radiation by the silicate particles in the dust plume [4][5]. The result of the directional filtering step will be a set of sub-images, each one of them contains image information at different orientations, the image dominant direction will be estimated based on the highest energy among the sub-images.

To locate dust clouds in a satellite image, we propose a segmentation technique that will connect dust cloud pixels in the satellite image. The method we use is based on the region growing algorithm [6]. We first start with a set of seed points obtained from the band math image Then these seed points will iteratively grow based on a criterion chosen to add pixels with similar gray level and that are connected to the region.

To locate dust sources, we use a corner detection method [7] to automatically locate corners in the dust cloud region, and then a carefully selected subset of these corners are declared to be the estimated dust source locations.

1.3 Earlier work and motivation

The motivation for our work was derived from methods and experiments documented in [4],[5],[8],[9],[10]. Most of these methods involved the use of band math analysis and assume that dark regions in the band math image are the dust cloud region, another research by Janugani et. al. involved the use of Principle Component Analysis (PCA) to detect dust clouds, Rivas-

Perea et. al. proposed a probabilistic model to detect dust clouds in MODIS images, while Chacon et. al. proposed the used of Artificial Neural Networks for the same purpose.

Regarding the prominent direction of dust clouds, Janugani et. al. proposed the use of the Discrete Fourier Transform (DFT) on blocks (Subregions) of the image, and then estimate the direction based on the orientation of the DFT spectrum of the block.

About the location of dust sources, Rivera-Rivera et. al. used the band math result image and manually locate dust sources based on prior knowledge of the geography of the region and the use of visual analysis. Also, Janugani et. al. used the results of false color composites of bands 1,4,and 5 to manually locate dust sources in the image.

1.4Thesis Overview

The rest of this thesis is organized as follows. Chapter two will focus our attention on locating the dust clouds and their sources. For locating dust clouds, we used the results of band math analysis as a preprocessing step to our method. We then perform binary thresholding of the resulting image. We perform this step to get a set of seed points that we will use in the region growing segmentation process. We first start the algorithm by growing the seed points by adding other points to the set if they match the connectivity and gray level closeness criterion chosen. The region will stop growing once there are no more points that can be added to the set. The region selected is considered to be one entity and it shares the properties of the seed points.

For detecting the dust cloud sources of transport matter, we will simply input the binary dust cloud image to a corner detection algorithm to locate convex corners in the image; these pixel locations can be assumed to be the automatically detected dust sources.

Chapter three will discuss the design and use of the Contourlet transform. We first briefly discuss the Fourier transform and some of its applications in image processing, and then we will mention its limitations and the need for better algorithms to increase the amount of information that can be acquired from the image. We then discuss the multi-resolution analysis, such as the Laplacian pyramid used in this thesis, and how it overcomes the limitations of the Fourier Transform by giving information in both spatial and frequency domains. After discussing the Laplacian pyramid, we will talk about directional filtering, a filtering technique that gives information about image texture orientation. Then we will discuss the combination of the Laplacian Pyramid and the directional filtering to create the state-of-the-art Contourlet transform. Then we will explain our use of the Laplacian pyramid as a preprocessing step to enhance the directional texture in the satellite images. We will then show how the directional filtering will help in estimating the dominant direction of the image. We will support our approach with an example image (Barbara).

In Chapter four we will discuss the future work that can be added to our research and summarize the conclusions.

CHAPTER 2

DUST CLOUD DETECTION AND SOURCE LOCATION

2.1 Dust Cloud Detection

2.1.1 Earlier work

Band math analysis has been used for detecting dust clouds in NOAA-AVHRR images by Rivera-Rivera [4] et. al. The band math is performed by taking the difference between band 4 and band 5. These two bands were chosen because there wavelengths highlight the absorption and subsequent emission of silicate particles in the dust cloud [5]. But the low signal to noise ratio of the acquired images may cause detection problems that will make it difficult for the band math to perform well.

The use of principle component analysis (PCA) was proposed by Janugani [9] et. al. to detect the dust clouds. K-means clustering analysis was also considered to detect the presence of dust clouds. The limitation in this method and the PCA results were not consistent and they work for a limited number of cases.

A probabilistic model was proposed by Rivas-Perea [8] et. al. to detect dust clouds. The proposed method was soil-independent and assumed that gray levels in the difference between bands 31 and 32 in MODIS images follows a Gaussian probability density function (PDF). The authors performed a Gaussian model parameter estimation (mean and variance), and the method was then used to preform segmentation by thresholding the PDF to a desired confidence interval. The method showed good promise, however, not all events can be assumed to behave like a Gaussian, and the method was restricted to work with MODIS images.

Another research by Chacon [10] et. al. involved the use of Artificial Neural Networks (ANN) to segment multispectral images. The proposed research showed good results in removing the water clouds from consideration and in reducing the computational burden. However, not all events were successfully detected.

2.1.2 Binary thresholding

Binary images are simply those whose pixels can take on only two values, 0 for black and 1 for white, and they are usually obtained from gray scale images through thresholding. Binary images have the advantage of having small memory requirements and their processing is faster. These types of images are used widely in computer vision applications for shape and property analysis [18].

One of the basic and simplest binary thresholding methods is hard thresholding, hard thresholding can be summarized with the following formula:

$$g(x) = \begin{cases} 0, f(x) < T \\ 1, f(x) > T \end{cases} \quad (1)$$

where f(x) is the input image and g(x) is the thresholded image, T is the threshold value.

In our research, we use instead hard thresholding in this way:

$$g(x) = \begin{cases} 1, band\ math < T \\ 0, band\ math > T \end{cases} \quad (2)$$

Because the dust region will be located at the smallest (negative) values of the band math image, this step was necessary to find the seed points needed for the region growing algorithm.

It has been considered in literature that the negative pixels obtained from the band math analysis are very likely to correspond to a dust cloud region [5]. However, not all negative values are accurately associated with a dust region. To illustrate, we show thresholding with T = 0 in Eq.(2)

for the event of Apr 15th 2003 on the right side of Fig 2.1, the left hand figure shows the result of thresholding using Eq. (2) with T is set to 0.

This example provided our motivation to find another method to locate dust clouds in a more accurate and automatic way. In our research, we propose the use of a region based segmentation technique to locate the dust cloud in a more accurate way, the method is called region growing. The region growing method used here starts by selecting a set of points, known as seed points, that share a set of properties (a specific range of gray levels in the band math image), the seed points region starts to expand if the neighboring pixels meet the criteria of growth, once the regions stops growing, the result is the new estimate of the dust storm region.

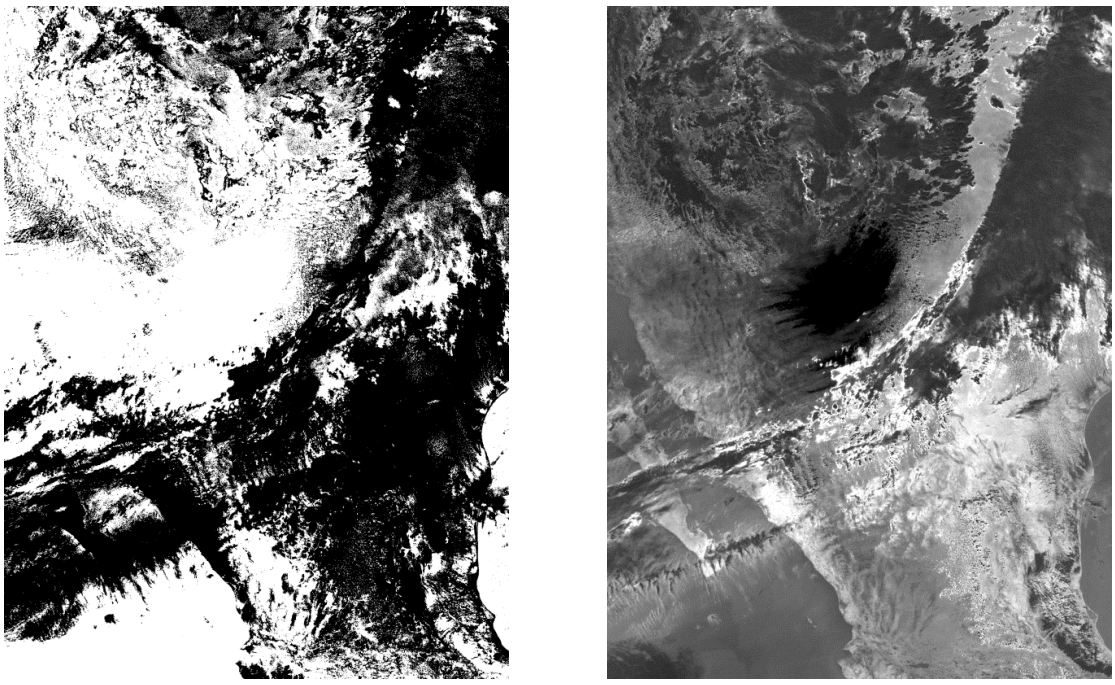

a b

Figure 2.1: a- Result of Bandmath analysis of bands 4 and 5 using Matlab, b – Bandmath analysis for the same bands using ENV

2.1.3 Image Segmentation based on the region growing algorithm

Region growing is a procedure that groups pixels or subregions into larger regions based on predefined criteria for growth [6]. To obtain the set of seed points, some prior information should exist. In our research, we used the result of bandmath analysis (using Matlab to allow for negative gray levels) and thresholded the result with a value less than 0, Figure 2.2 shows the result of thresholding with a value of -11.

Figure 2.2: Result of threshold the bandmath image with a value less than 0.

Now to obtain a minimal number of seed points, the thresholded bandmath image was applied into a shrinking process, so that each connected component will shrink into a point. The shrinking is a standard Matlab morphological operation. Then we apply the region growing algorithm into the bandmath image using the set of seed points obtained from above. The criterion to add new pixels was the difference in gray level values, the selection of this parameter

(difference in gray level value) was chosen manually since it depends on the nature of the problem. For this event, the parameter value is 43. The result of the segmentation is shown in Figure 2.3 and then used in Fig. 2.4 to better illustrate the results.

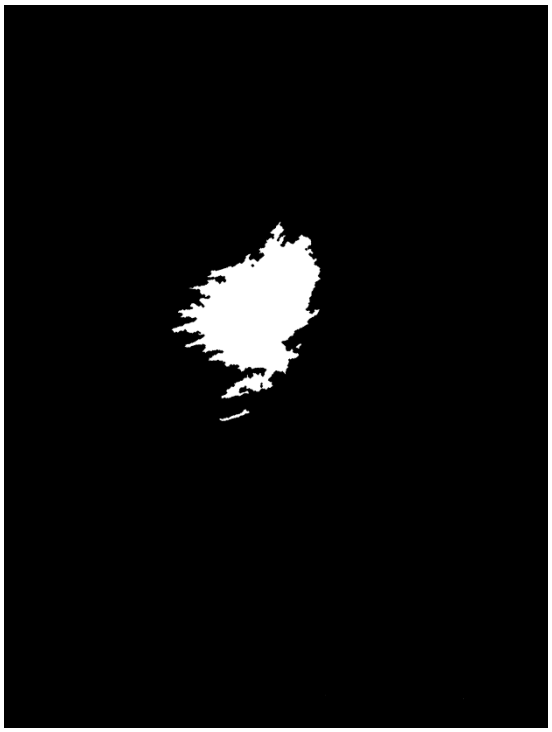

Figure 2.3: The result of image segmentation based on the region growing

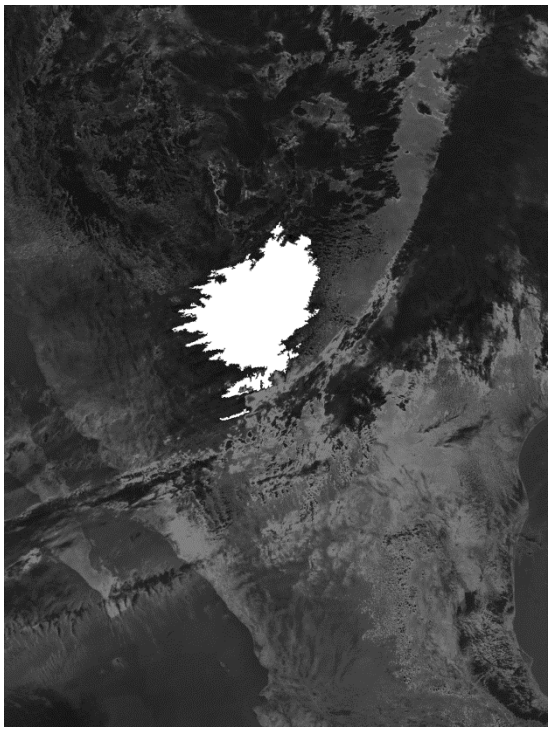

Figure 2.4: The segmented image superimposed into the satellite image.

2.1.4 Experimental Results

We focused our research on 4 events, the known dust storm events were: Apr 15th 2003, Dec 15th 2003, Dec 26th 2003, and Mar 04th 2003. Most of these events were used in other studies such as [9][11]. The steps we followed for each event were:

1 – Obtain the band math image by taking the difference between bands 4 and 5.

2 – Threshold the resulting image using Equation (2), the negative threshold value is event dependent and selected by the user.

3 – Apply the Region Growing Algorithm using result obtained in step 2.

2.1.4.1 Apr 15th 2003 event

Figure. 2.5 below shows both bands 4 and 5 of the Apr 15th 2003 satellite image.

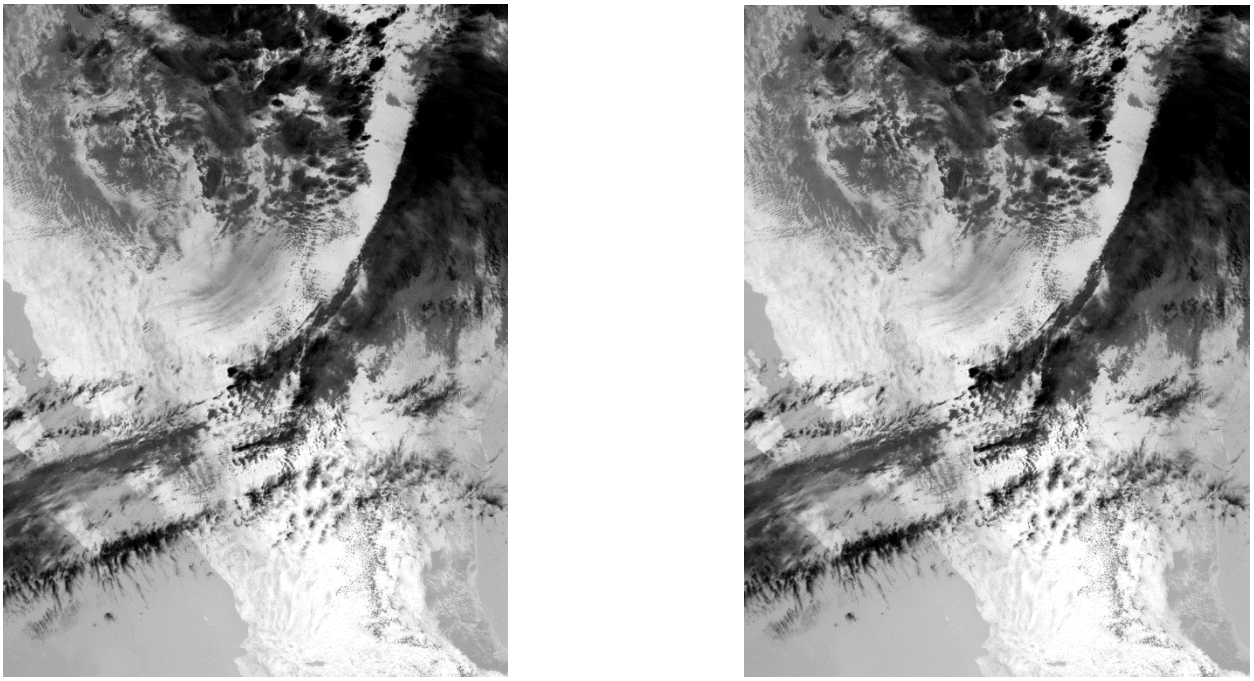

Fig 2.5: Bands 4(left) and 5(right) of the satellite image of Apr 15th 2003 event.

The resulting band math image (Band 4 minus Band 5) is shown in Figure 2.6

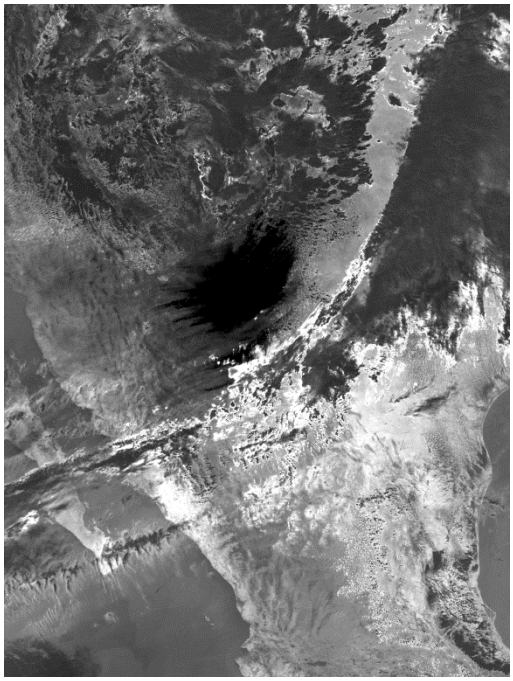

Fig 2.6: Band Math image of the Apr 15th 2003 event.

We then threshold the band math image using Eq. (2) with a value for T of -11. The result of this step is shown in Fig 2.7

Fig 2.7: the thresholded band math image obtained using Eq. (2) for Apr 15th event.

After the previously described shrinking process, we obtain the set of seed points from the thresholded band math image. We then apply the region growing algorithm starting with this set of seed points; the result obtained is shown in Figure 2.8

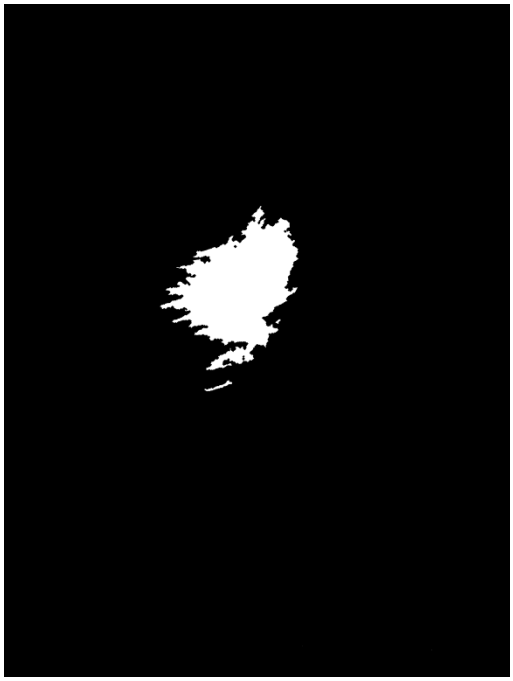

Fig 2.8: The result of image segmentation for Apr 15th event.

2.1.4.2 Dec 15th 2003 event

Figure 2.9 shows both bands 4 and 5 of the Dec 15th 2003 NOAA-AVHRR satellite image.

Fig 2.9: Bands 4(left) and 5(right) of the satellite image of Dec 15th 2003 event.

The resulting band math image is shown in Figure 2.10

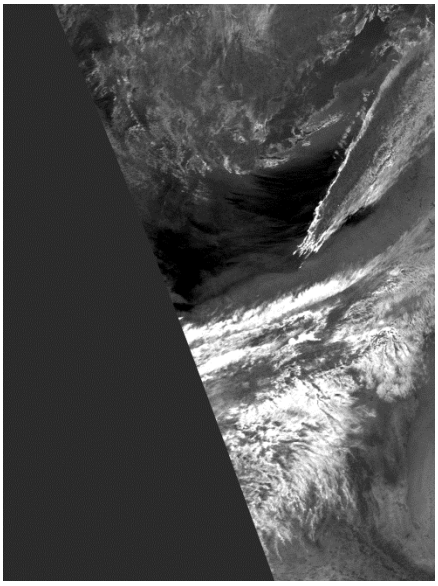

Fig 2.10: Band Math image of the Dec 15th 2003 event.

We then threshold the band math image using Eq. (2) with the value for T of -5. The result of this step is shown in Fig 2.11

Fig 2.11: The thresholded band math image obtained using Eq. (2) for Dec 15th event.

We then apply the Region Growing algorithm to the thresholded band math image using the set of seed points obtained after the shrinking process, the result obtained is shown in Fig 2.12

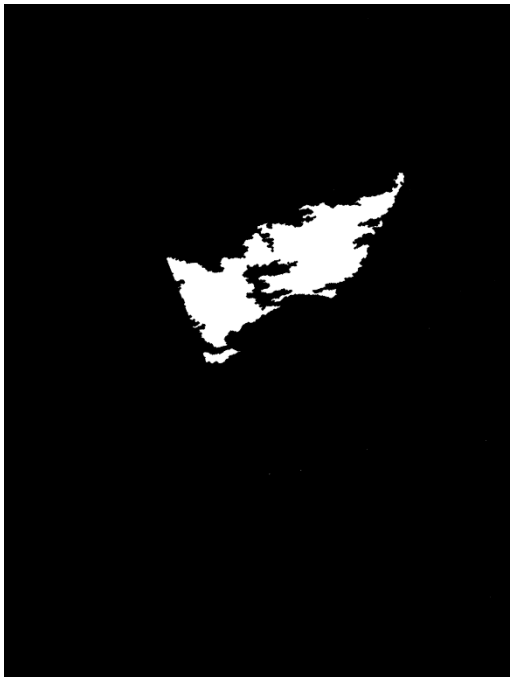

Fig 2.12: The result of image segmentation for Dec 15th event.

2.1.4.3 Dec 26th 2003 event

Figure. 2.13 shows both bands 4 and 5 of the Dec 26th 2003 NOAA-AVHRR satellite image.

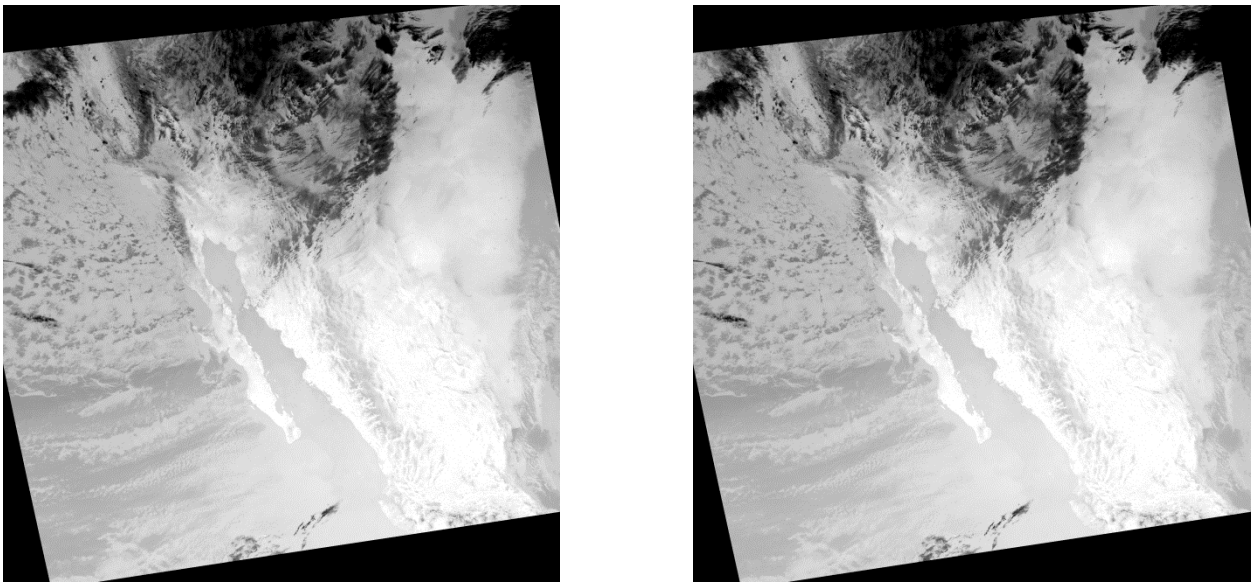

Fig 2.13: Bands 4(left) and 5(right) of the satellite image of Dec 26th 2003 event.

The resulting band math image is shown in Figure 2.14

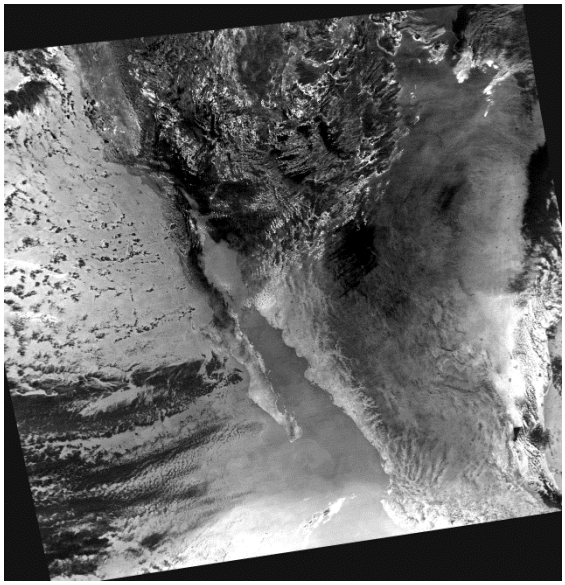

Fig 2.14: the band math image of Dec 26th event

The thresholded band math image using Eq. (2) with T = -10 is shown in Fig 2.15

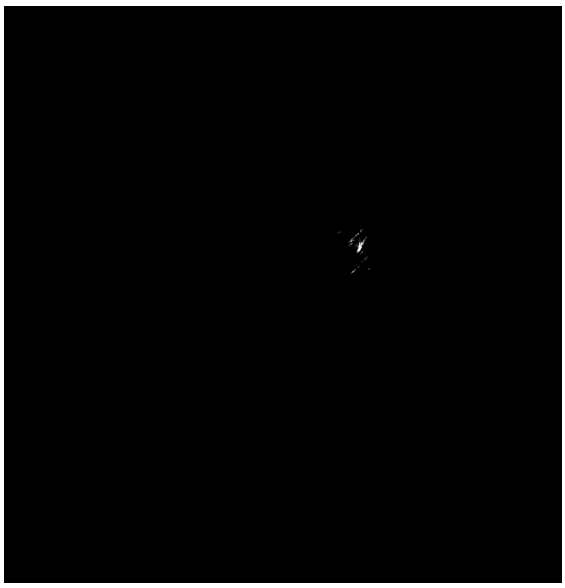

Fig 2.15: The thresholded band math image obtained using Eq. (2) for Dec 26th event.

We then apply the Region growing algorithm to the thresholded band math image using this set of seed points, the result obtained is shown in Fig 2.16

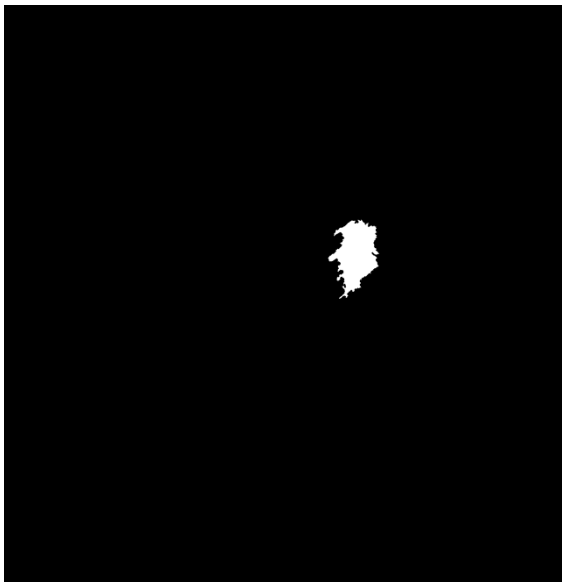

Fig 2.16: The result of image segmentation for Dec 26th event

2.1.4.4 Mar 04th 2003 event

Figure 2.17 shows both bands 4 and 5 of the Mat 04th 2003 satellite image.

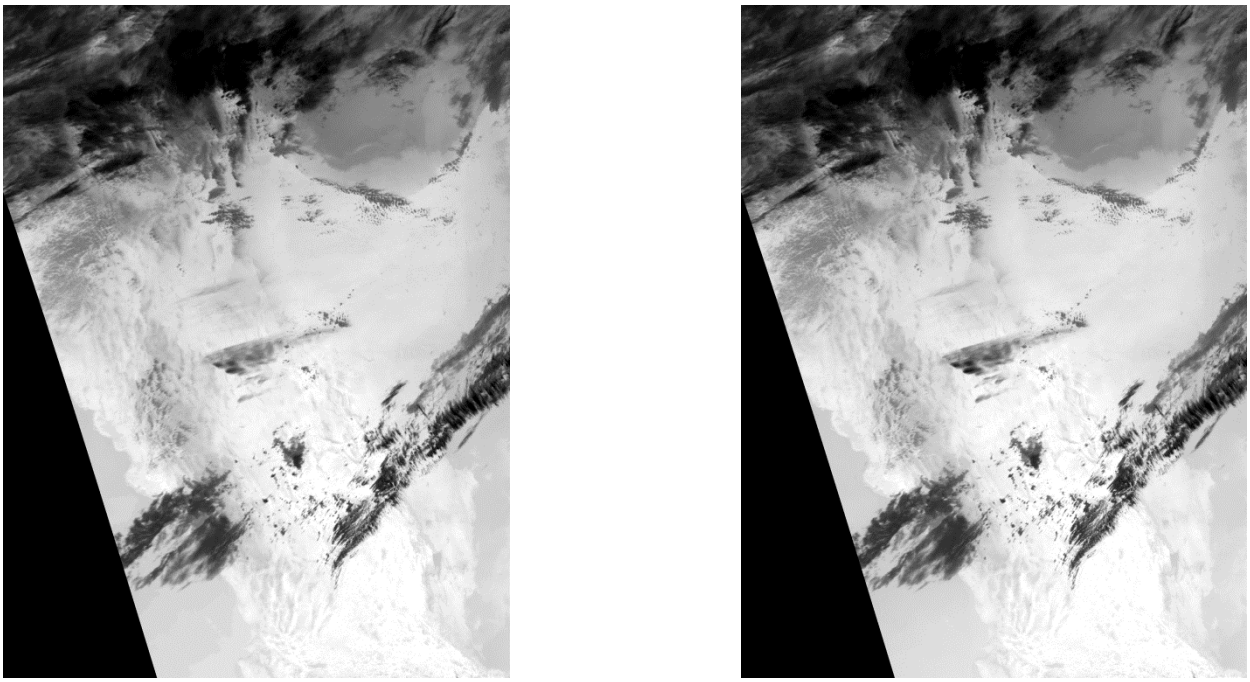

Fig 2.17: Bands 4(left) and 5(right) of the satellite image of Mar 04th 2003 event.

The resulting band math image is shown in Figure 2.18

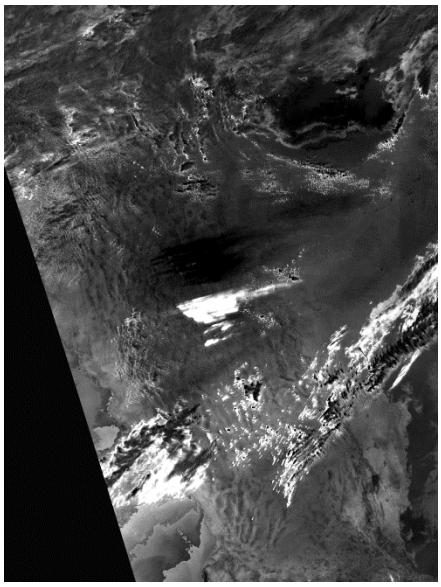

Fig 2.18: The band math image of Mar 04th event

Thresholding the band math image using Eq. (2) with value of T equal to -12, gives the result shown Fig 2.19

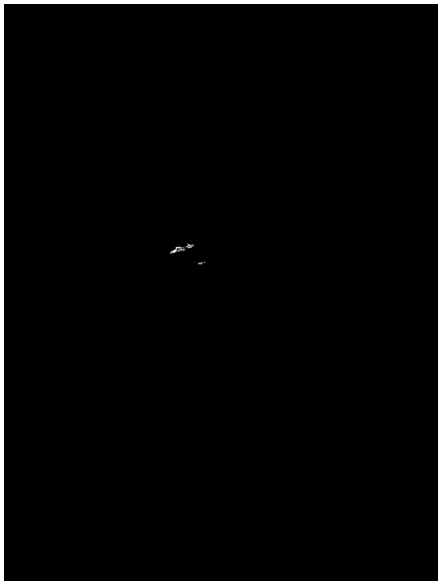

Fig 2.19: The thresholded band math image obtained using Eq. (2) for Mar 04th event.

The Region growing algorithm gives the result shown in Fig 2.20

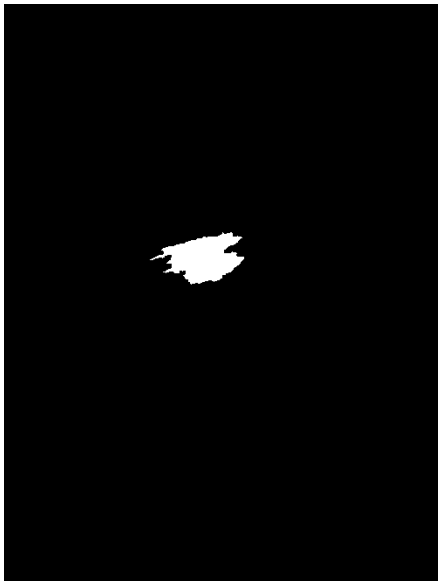

Fig 2.20: The result of image segmentation for Mar 04th event.

2.2 Dust Sources Location

2.2.1 Earlier Work

Several Studies have been conducted to locate dust cloud sources in satellite images, Rivera-Rivera et.al. used a priori knowledge of the area geography [11] to locate and characterize dust sources. The dust sources were located manually based on the user input and thus was not automatic.

Janugani et. al. addressed the problem of locating dust sources by using false color composites of bands 1, 4, and 5 in NOAA-AVHRR images. The resulting image was an enhanced image that makes it easier for the eye to visually locate dust sources.

Since neither of the methods above were automatic, this gave us a motivation to find a method to automatically locate dust sources on the same type of satellite images.

2.2.2 Polygonal Approximation

After detecting the dust clouds using the segmentation technique described in section 2.1, we propose an additional processing to locate dust sources automatically. The method involves the use of corner detection to locate corners on the boundary of the segmented region obtained before; however, for some events the image boundary has too much detail that causes us to detect even small corners that cannot be important dust sources. In order to avoid this issue, we used a method to simplify the image boundary and to represent this perimeter-contour with less number of segments. The goal for this step is to capture the essence of the shape in a given boundary using a reduced number of segments; one of the most powerful methods finds a minimum-perimeter polygon (MPP).

The first step for the MPP algorithm is to enclose the boundary of the image by a sequence of cells, as shown in Figures 11.6 and 11.7 in [6]. Now by assuming that the boundary is like a rubber band that can shrink, it will be constrained by the inner and outer walls of the region defined by the cells. The algorithm can be simplified by obtaining the convex and concave points in the region enclosed by the cells, as in Fig 11.7 b in reference [6], we then displace the concave points to their diagonal mirror locations in the outer wall of the bounding region while keeping the convex points unchanged. Finally, we simply connect the set of displaced concave points and the unchanged convex points.

Fig, 2.24 shows the set of images illustrating the use of polygonal approximation on a binary image for different cell sizes.

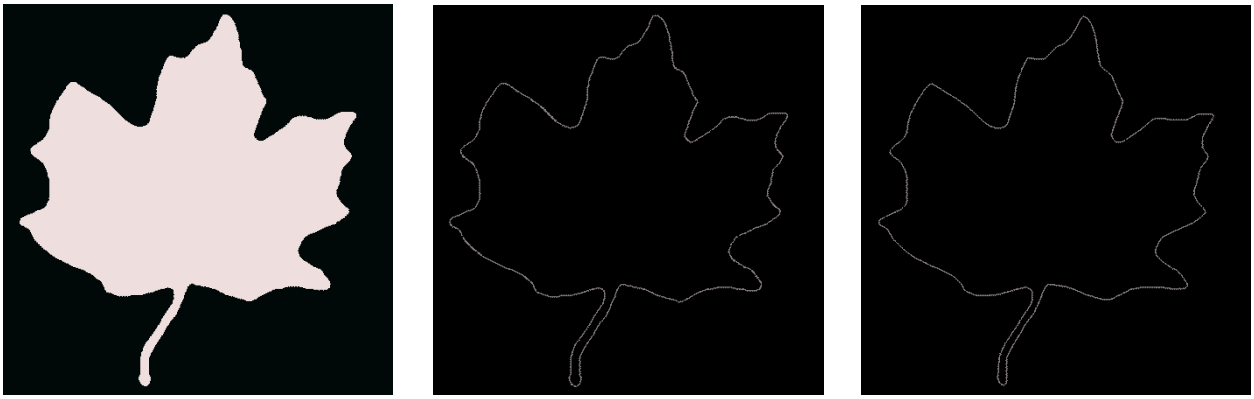

(a) (b) (c)

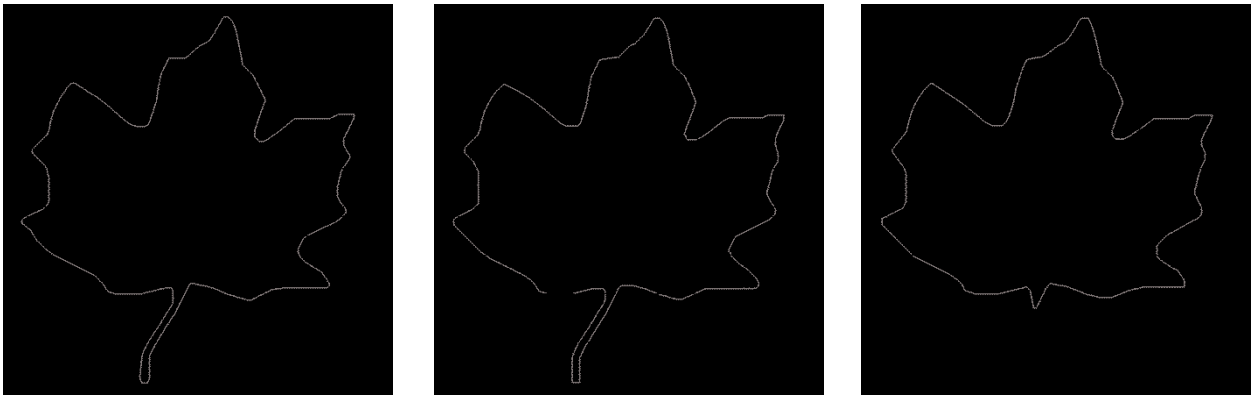

(d) (e) (f)

Fig 2.24: (a) Original binary image. (b) The boundary of the image. (c) Through (f) MMPs obtained using square cells of sizes 2, 3, 4, and 5, respectively.

2.2.3 The Harris corner detector

A corner can be defined as a pixel in a small neighborhood where two dominant and different edge directions meet, it can also be identified in a simpler way as a junction of contours.

The Harris corner detector [7],[12] is an improved method that considers the differential of the corner score (sum of squared differences). By considering a 2D gray-scale image f, an image patch is taken and shifted by Δx, Δy. The windowed sum of square differences between values of the image f and its version is given by:

$$S(\Delta x, \Delta y) = \sum_{x,y} W(x,y)\,[f(x,y) - f(x-\Delta x, y-\Delta y)]^2 \quad (3)$$

The corner point must have a high response value of S(Δx,Δy). If the shifted image patch $f(x-\Delta x, y-\Delta y)$ can be approximated by the first Taylor expansion

$$f(x-\Delta x, y-\Delta y) \approx f(x,y) + \left[\frac{\partial f(x,y)}{\partial x}, \frac{\partial f(x,y)}{\partial y}\right]\begin{bmatrix}\Delta x \\ \Delta y\end{bmatrix} \quad (4)$$

By Substituting (4) into (3) we obtain:

$$S(\Delta x, \Delta y) = \sum_{x,y} W(x,y)\,\left(\left[\frac{\partial f(x,y)}{\partial x}, \frac{\partial f(x,y)}{\partial y}\right]\begin{bmatrix}\Delta x \\ \Delta y\end{bmatrix}\right)^2 \quad (5)$$

Having in mind that $U^2 = U^T U$, equation (5) will be

$$S(\Delta x, \Delta y) = \sum_{x,y} W(x,y)[\Delta x, \Delta y]\left(\begin{bmatrix}\frac{\partial f}{\partial x} \\ \frac{\partial f}{\partial y}\end{bmatrix}\begin{bmatrix}\frac{\partial f}{\partial x} & \frac{\partial f}{\partial y}\end{bmatrix}\right)\begin{bmatrix}\Delta x \\ \Delta y\end{bmatrix}$$

$$S(\Delta x, \Delta y) = [\Delta x, \Delta y]\left(\sum_{x,y} W(x,y)\left(\begin{bmatrix}\frac{\partial f}{\partial x} \\ \frac{\partial f}{\partial y}\end{bmatrix}\begin{bmatrix}\frac{\partial f}{\partial x} & \frac{\partial f}{\partial y}\end{bmatrix}\right)\right)\begin{bmatrix}\Delta x \\ \Delta y\end{bmatrix}$$

$$S(\Delta x, \Delta y) = [\Delta x, \Delta y]\, A_w(x,y)\begin{bmatrix}\Delta x \\ \Delta y\end{bmatrix}$$

Where $A_W(x,y)$ is known as the Harris matrix and given by:

$$A_W(x,y) = \sum_{x,y} W(x,y)\left(\begin{bmatrix}\frac{\partial f}{\partial x} \\ \frac{\partial f}{\partial y}\end{bmatrix}\begin{bmatrix}\frac{\partial f}{\partial x} & \frac{\partial f}{\partial y}\end{bmatrix}\right)$$

The small window W(x,y) can be 1 valued as a simple case, but usually a Gaussian window is used. The main modes of the Harris matrix are reflected in the eigenvalues λ_1, λ_2. These modes of variation can be found using principle component analysis. Three distinct cases are of interest:

1 – Both eigenvalues are small. This means that image f is flat in the examined pixel neighborhood.

2 – One eigenvalue is small and the other is large. The local neighborhood is ridge shaped.

3 – Both eigenvalues are large. A small shift in any direction causes significant change of image f. A corner is detected in this case.

The Harris corner detector has been very popular. Its advantages are insensitivity to 2D shifts and rotations, and low computational requirements [12].

2.2.4 Experimental Results

We focused our research on three events to locate dust sources, the events of interest are Apr 15th 2003, Dec 26th 2003, and Mar 04th 2003. The Dec 15th 2003 was not suitable to apply our method on it since the dust sources region was cut from the satellite image.

The events that needed the polygon approximation were the Apr 15th 2003, and the Dec 26th 2003, since the boundary of the segmented region has a lot of small corners that might affect the performance of the corner detection method.

2.2.4.1 Apr 15th 2003 event

We first simplify the image by using the MMP method and the result obtained are shown in Fig 2.25

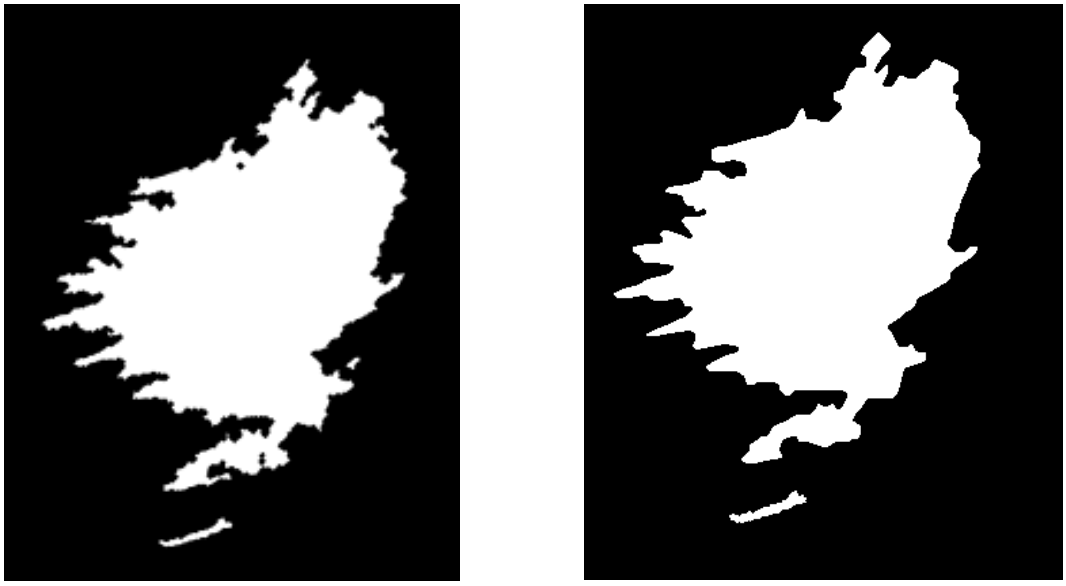

Fig 2.25: the original dust cloud region for Apr 15th event (left) and its polygonal simplified version (right) for Apr 15th event.

For this image we used a cell size of 2, since we don't want to lose too much details of region boundary. The main purpose of using MPP is to smooth the image boundary, and thus we applied the smallest cell size.

After smoothing the image and removing the small details in the boundary, we apply the corner detection algorithm. The results are shown in Fig 2.26

Fig 2.26: The results of the corner detection method for Apr 15th event.

It is clear that not all corners can be assumed to be dust sources, so we propose a post-processing method to remove the points that should not belong to the set of dust sources. The method consists of two steps:

1 – Remove the concave points; since they should not belong to the set of dust sources.

2 – Determine if sources are on the left (west) or right (east) side. To do this, we will find the centroid of the binary region that represents the dust cloud region, then we divide the region into

two sub-regions using a vertical line that crosses the centroid point, and then we find the length of the perimeter at each sub-region, the perimeter with highest length is assumed to be the one that contains dust sources.

Step one can be easily implemented by applying a square window of an arbitrary odd size centered at each corner point. Next calculate the area of the filled region inside the square, we then have two cases:

a - If the area is larger than 50% of the square area, then the point is a concave and is not a dust source.

b – If the area is less than 50% of the square area, the point is a convex and considered to be a dust source.

After applying this method we obtained this result shown in Fig 2.27.

We then apply step 2 to the resulting set of points, we first find the centroid of the perimeter $(\bar{r},\bar{c})$ and then separate the dust cloud region into two sub-region, the result is shown in Fig 2.28, the values of $(\bar{r},\bar{c})$ are given by

$$\bar{r} = \frac{1}{A}\sum_{r=0}^{N-1}\sum_{c=0}^{N-1} rf(r,c)$$

$$\bar{c} = \frac{1}{A}\sum_{r=0}^{N-1}\sum_{c=0}^{N-1} cf(r,c)$$

where A is the area of the binary region enclosed in a square of size N×N. Results are shown in figures 2.27 and 2.28

Fig 2.27: the selected corners that passed step one of Apr 15th event.

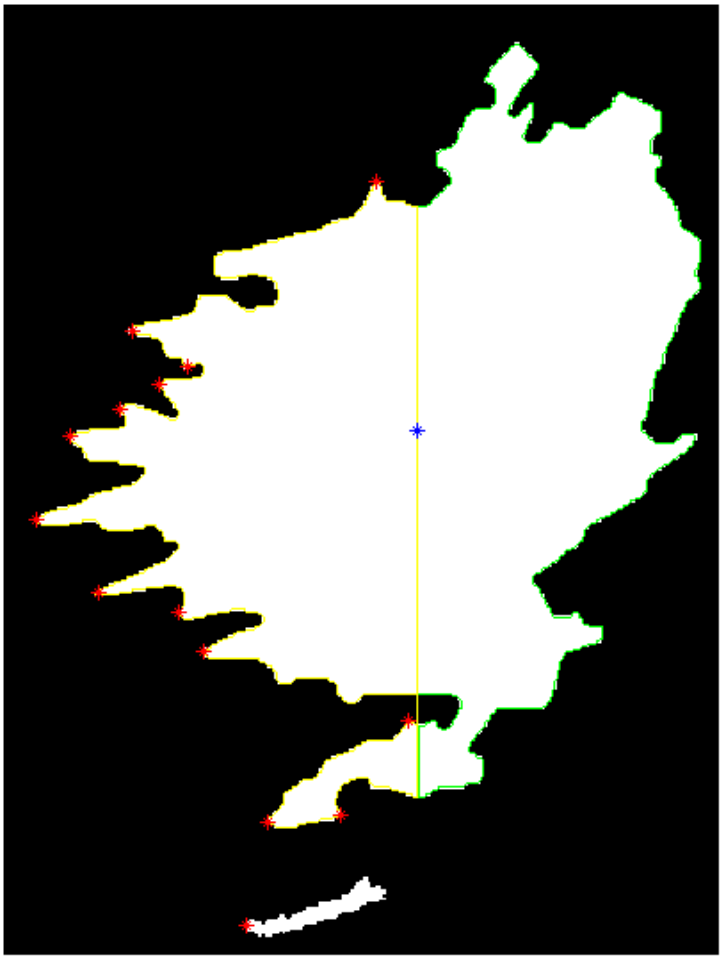

Fig 2.28: the selected corners that passed step two of Apr 15th event.

The blue spot at the middle is the centroid of the binary image, while the red spots are assumed to be the dust sources, the yellow and green lines are the contours of the 2 sub-regions separated by the line generated at the centroid. The length of the yellow line was 838 while the green line was 622, so it's assumed that the region enclosed by the yellow line (west/left side) contains the dust sources.

2.2.4.2 Dec 26th 2003 event

Similar analysis has been done here and the result of the MPP is shown in Fig 2.29

Fig 2.29: the original dust cloud region of Dec 26th event (left) and its polygonal simplified version (right)

We next obtain the set of corners and process them as before as shown in Fig. 2.30. The blue point represents the centroid of the binary region, the length of the yellow line is 281, and the length of the green line is 219, so the set of corners (the red spots) are assumed to be on the yellow line (left/west).

Fig 2.30: the selected corners after passing steps one and two for Dec 26th event.

2.2.4.3 Mar 04th 2003 event

For this event, we did not use the MPP method since it was not necessary to simplify the boundary, the results for corner detection are shown in Fig 2.31

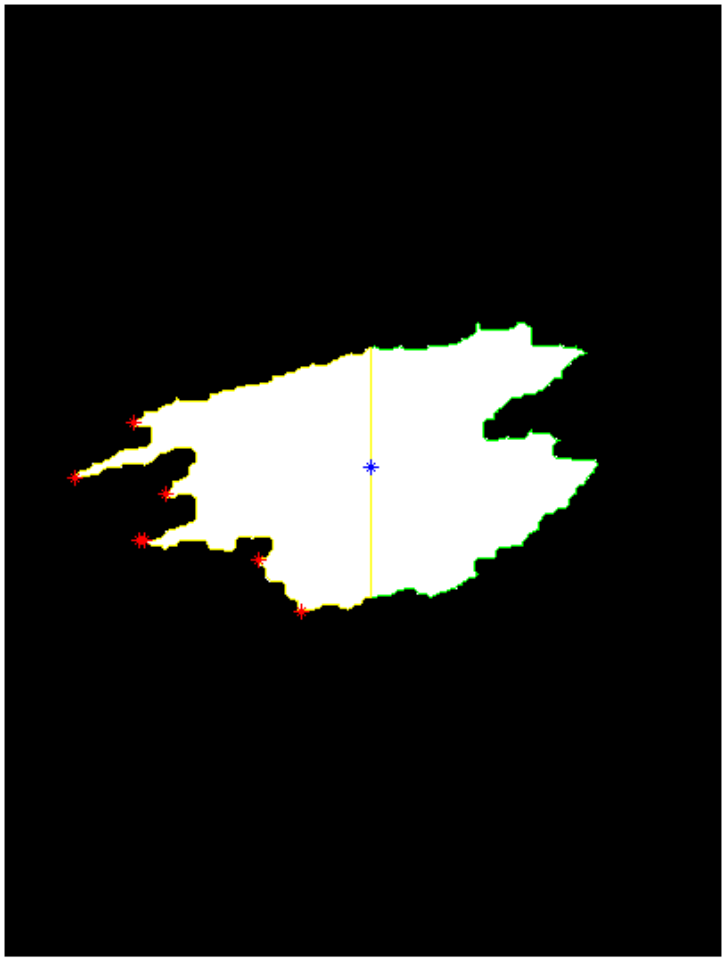

Fig 2.31: the selected corners after passing steps one and two.

The length of the green line is 669, and the length of the yellow line is 805, so the dust sources were expected to be on the yellow line (West/Left).

2.2.4.4 Summary on the results

In this section, we will show the corners and there location on the satellite image

1 – The Apr 15th 2003 event is shown in Fig. 2.32

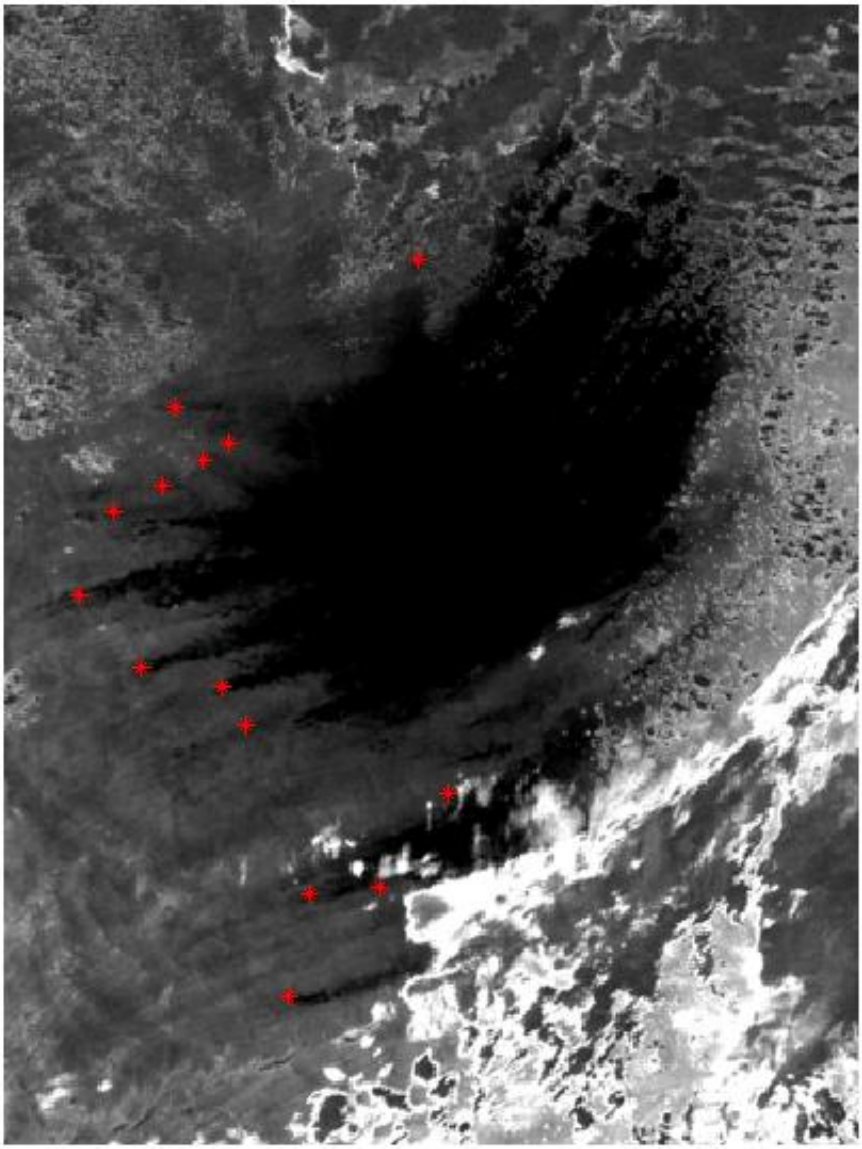

Fig 2.32: the location of dust sources in the satellite image for Apr 15th event.

2 – The Dec 26th 2003 event is shown in Fig. 2. 33.

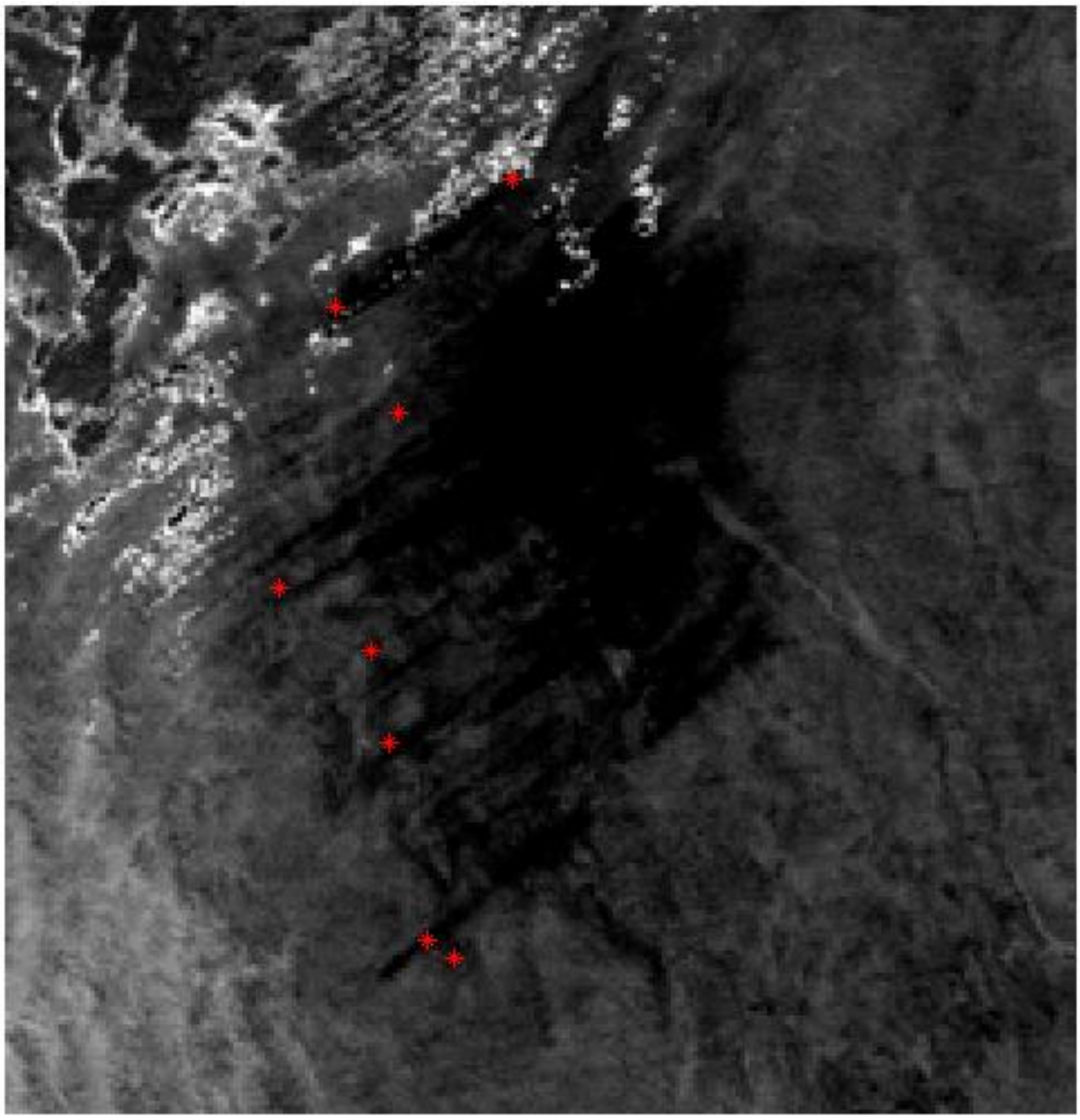

Fig 2.33: the location of dust sources in the satellite image for Dec 26th event.

3 – The Mar 04th 2003 event is shown in Fig. 2.34

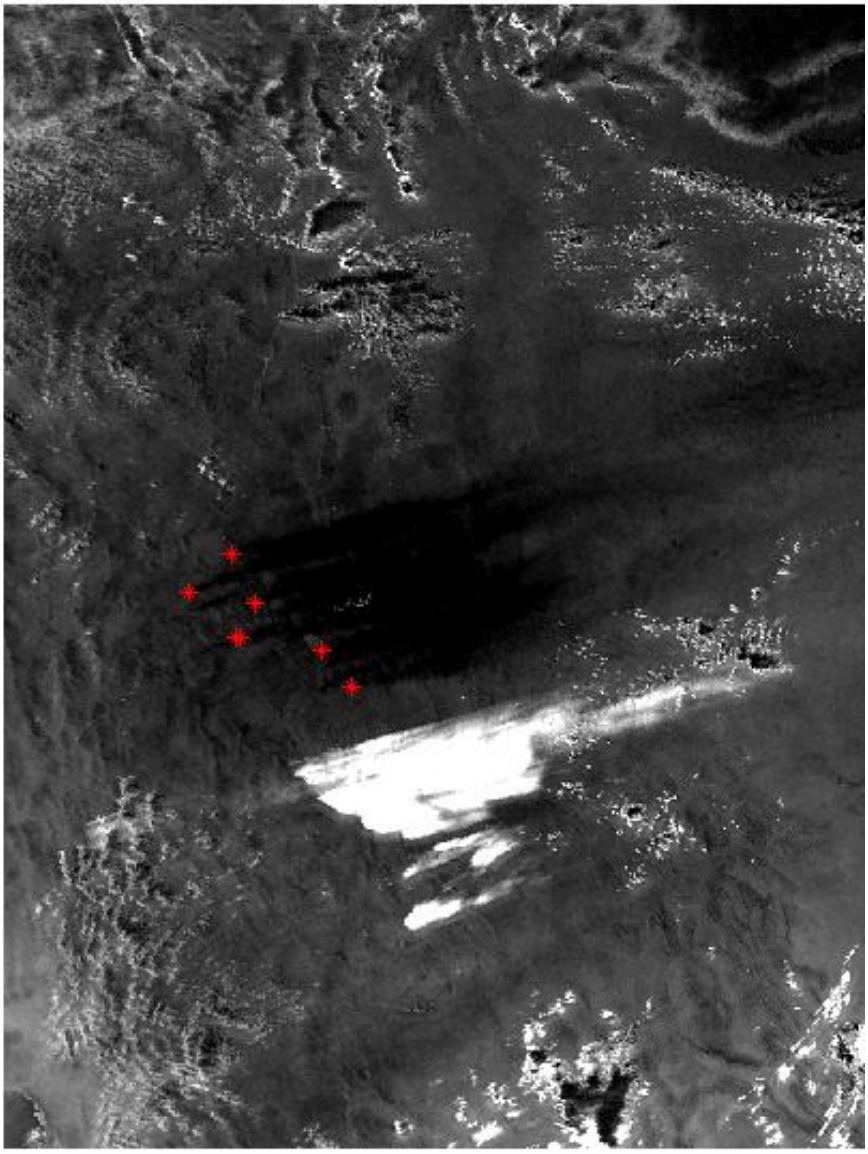

Fig 2.34: the location of dust sources in the satellite image for Mar 04th event.

CHAPTER 3

ESTIMATING THE DIRECTION OF MOTION OF DUST CLOUDS IN NOAA-AVHRR SATELLITE IMAGES

3.1Earlier work

The motivation for our work was derived from the experiments documented in [9]. The methodology developed in that paper involved the use of band math analysis and principle component analysis to detect the dust clouds, their method also involves the use of edge detection techniques followed by false color composition to detect the dust sources visually. After they confirm the presence of a dust cloud, that region is applied to a sequence of image processing steps, such as power spectrum analysis, binary thresholding, and morphological operations, to estimate the transport direction of the dust storm, however, the results suffered from lack of high precision and consistency.

3.2 The Contourlet transform

The Contourlet transform [13] is a two-dimensional representation for images that can capture the geometrical structure of pictorial information, see chapter 4 in [14]. It consists of a double filter bank structure, known as *pyramidal directional filter bank*, by combining the Laplacian pyramid [15] with a directional filter bank [16]. This provides a flexible multi-resolution and directional decomposition for images. However, for the purpose of our research, we used the elements of the Contourlet transform separately; the block diagram in Fig. 3.1 illustrates our use of the Contourlet transform.

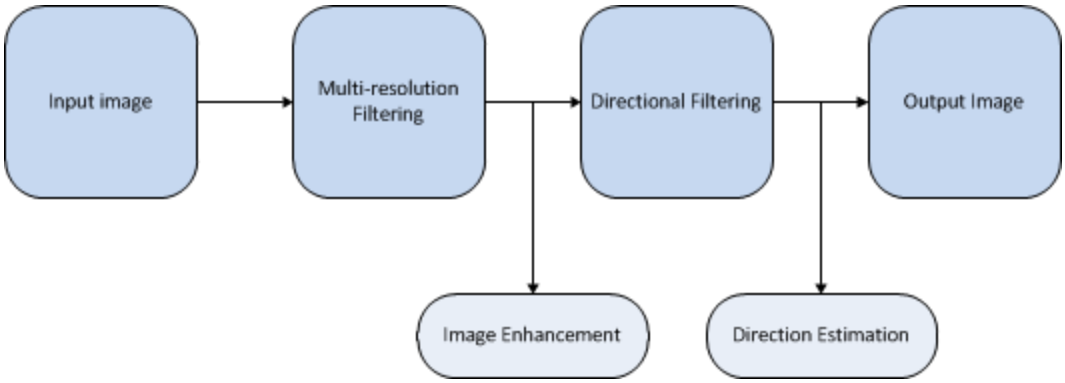

Fig 3.1: The use of the Contourlet transform elements for estimating the direction of motion in dust clouds.

From the above block diagram, we applied the image into the Laplacian pyramid, and then amplified the high frequency coefficients; the reason for this step is that the high frequency coefficients contain information about the edges of the image. Most of the desired information is in the form of edges, so by doing this step, we enhance the image before the directional filtering.

We next apply the enhanced image to a directional filter, the output of this step is a set of images, each one contains information about the image in a specific direction. We then measure the energy of each image, and assume the one with the highest energy is the one with the prominent direction. This whole process is done on a block-by-block basis in order to obtain the prominent direction for each small patch (block) of the whole dust cloud image.

The block diagram of Fig. 3.2 shows in more details how we used the Contourlet transform for our research.

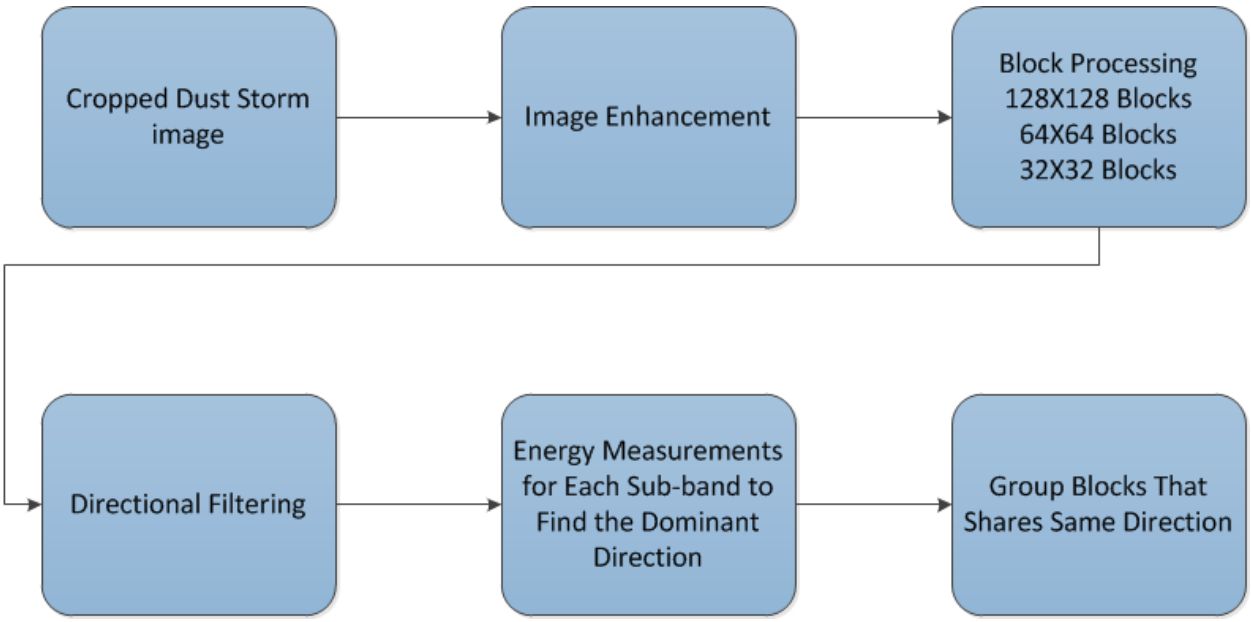

Fig 3.2: the system used to find the dominant direction.

The reason for cropping the image is to use our prior knowledge of the location of the dust cloud and to reduce the computational burden. In the following sections, we explain briefly the use of both the Laplacian pyramid and the directional filter and their application in our research.

3.2.1 The Laplacian Pyramidal

In this research, we used the Laplacian pyramid as a preprocessing step for image enhancement before applying it to a directional filter, this step is necessary to strengthen the directional streaks on the dust cloud image to improve the performance of the directional filter. The block diagram of Fig. 3.3 shows in detail how we used the Laplacian pyramid for image enhancement.

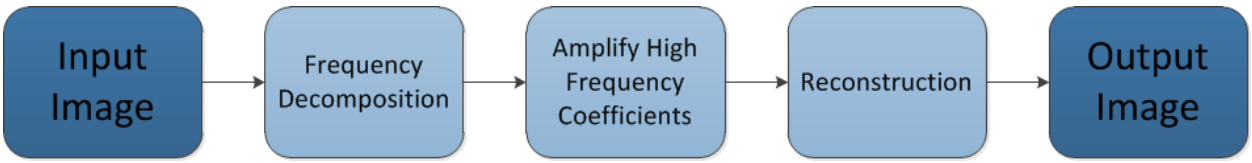

Fig 3.3: Block diagram used for image enhancement.

We first decompose the image into sub-bands; the ideal frequency response of the Laplacian pyramid is shown in Figure 3.4. Each sub-band has different information from the image, the lower index sub-bands correspond to higher frequency components, and they contain the information about sharp edges. The highest index sub-band corresponds to the lowest frequency region, and it has information about the smooth variations of the image gray levels.

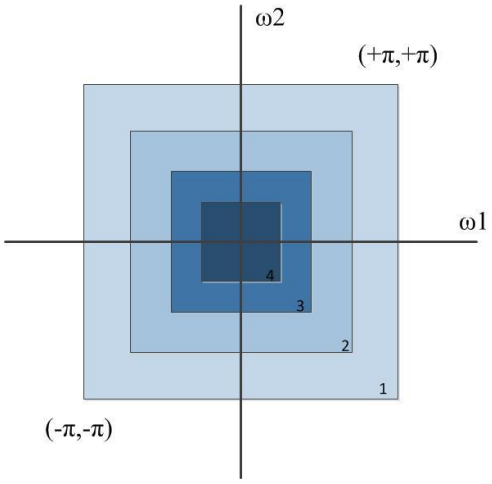

Fig 3.4: frequency divisions of non-subsampled Laplacian Pyramid.

Since we want to enhance the sharp edges of the image, we will amplify all sub-bands, except the one with the highest index, since they have the information about the directional streaks that appear in the dust storm part of the image. The amplification will be done by multiplying the high frequency sub-bands with a factor larger than one [17]. After doing this step, we reconstruct the image from the modified sub-bands to get an enhanced version of the original image.

As an example, we applied the previous approach on the well-known Barbara image. The image was chosen, since it has many regions with well-defined directional texture. We used an amplification factor of 2, and 4 levels of decomposition as illustrated in Fig. 3.5.

Fig 3.5: Original Barbara image (Left), an Enhance image (right)

3.2.2 Directional Filtering

Directional Filtering is a very significant tool in many image processing applications such as feature extraction, texture analysis, and object recognition. In this research, we used the non-subsampled directional filter bank (NSDFB) documented in [13] to find the dominant direction of the dust storm. The NSDFB divides the image into sub-bands based on their orientation and the number of sub-bands, which is related to the number of levels by this equation:

$$L = 2^n$$

L: Number of sub-bands.
n: number of levels

The ideal frequency response of a 2-level NSDFB is shown in Fig. 3.6.

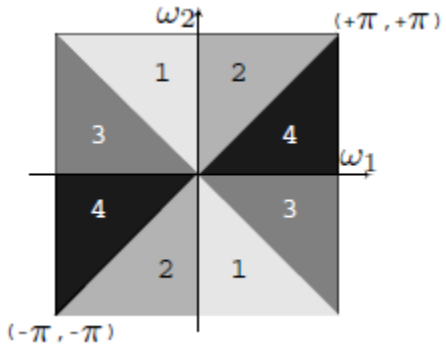

Fig 3.6: Frequency divisions of 2-level NSDFB.

As an illustration of directional filtering, we applied a small image patch into the 4-level directional decomposition. The result we obtained are shown in Fig 3.7

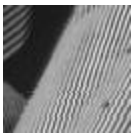

(a)

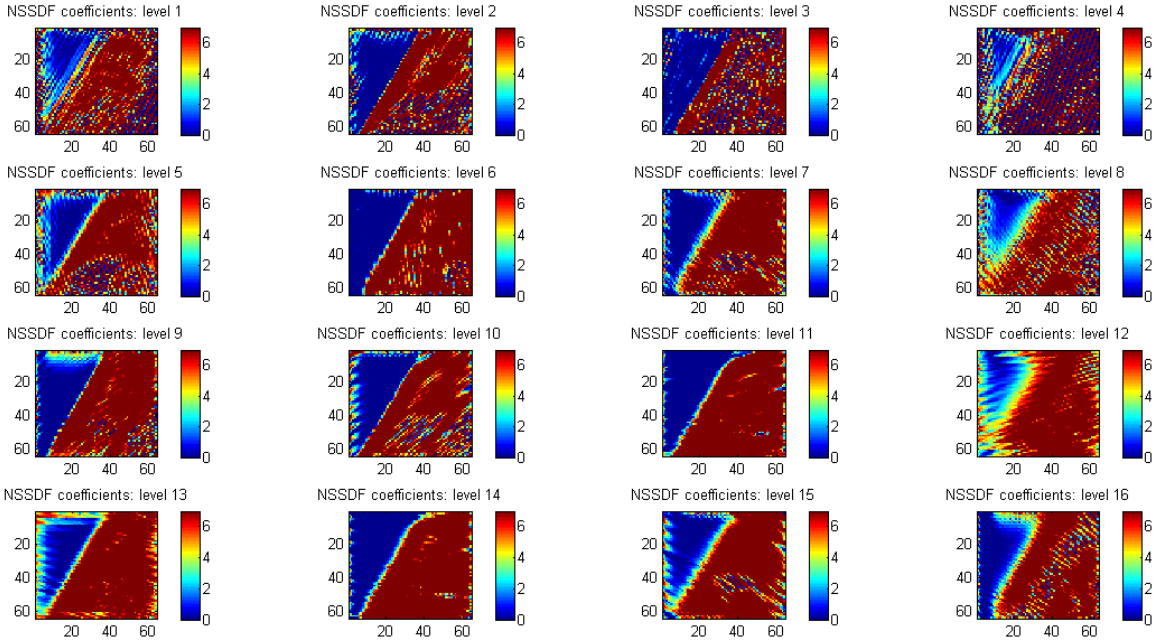

(b)

Fig 3.7: (a) Sample image. (b) 4 level directional decomposition

From the above example, it was hard to visually tell which sub-band contains the dominant direction; instead, we made an objective decision by computing the energy for all sub-bands in order to choose the prominent direction automatically. For this specific example, the dominant angle took the ranges of 67.5° – 78.75°. Since the maximum we can get is 16 sub-bands for the image sizes used in our examples, the angle range will be from 0° - 180° in steps of 180°/16 = 11.25° for each sub-band.

3.3 Block Processing

The block Processing is used to divide the image into a set of blocks of a small size (32X32 or 64X64) in order to perform the directional filtering for each block individually. The block processing is essential since the dust cloud does not occupy the whole space in the satellite image and the direction may vary spatially. After applying the directional filtering, we will focus on the blocks that are in the dust cloud region. Having a set of blocks that have the same prominent direction means that the blocks belong to the same subset of a dust cloud. This can be used as a confirmation of the presence of a dust cloud.

As an example, we applied the combination of block processing and directional filtering on the Barbara image which has a lot of directionality. The results we obtain are shown red arrows on the image, the direction of the arrow indicates the prominent direction of the block in the range 0°-180°, leaving an inherent ambiguity of 180° in the actual direction. The result we got is shown in Fig. 3.8

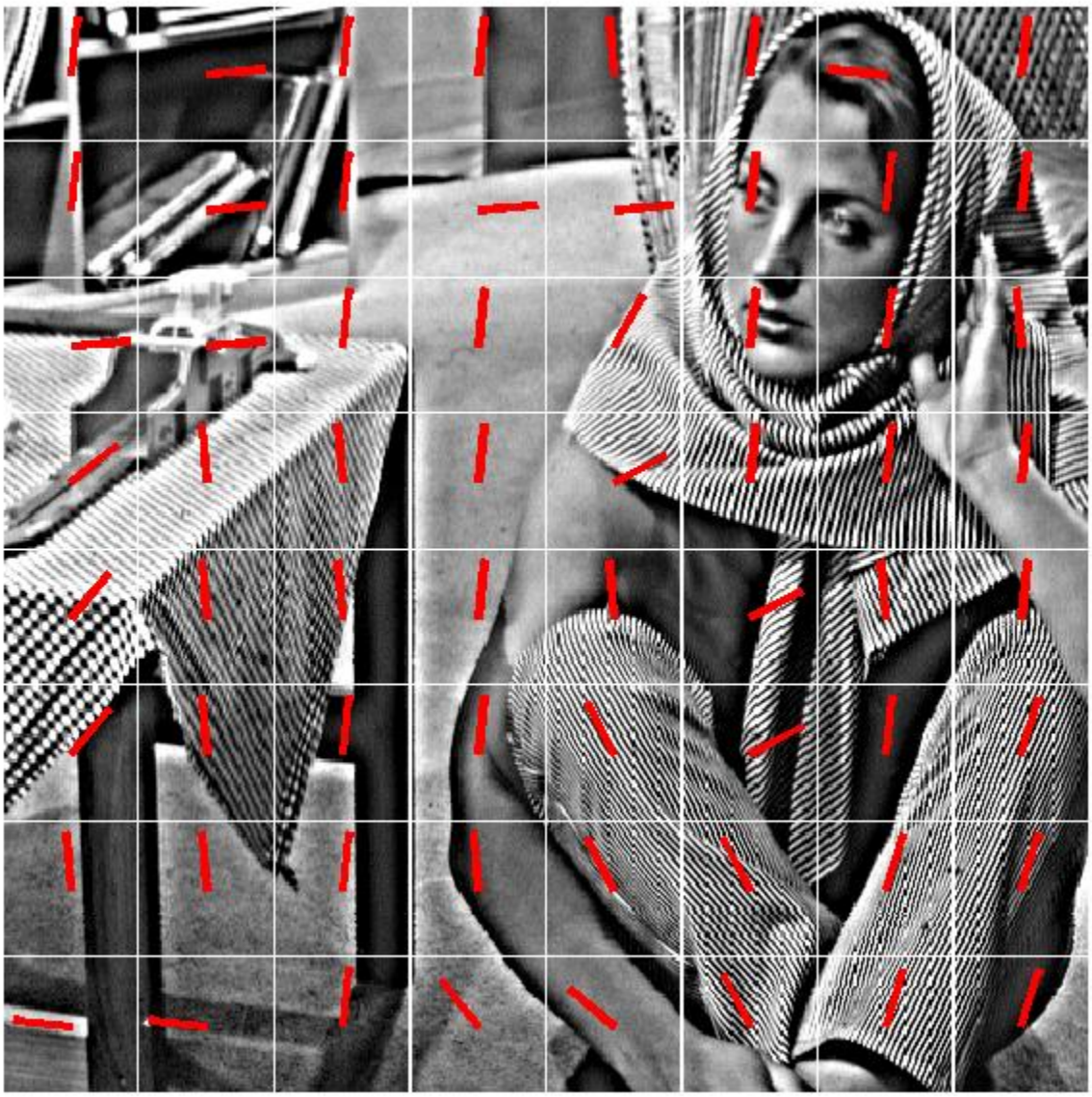

Fig 3.8: the result of directional filtering and angle estimation applied to separate blocks of the Barbara image.

3.4 Experimental results.

We focused on the same set of data we used in chapter 2; but we first crop the part of the image that contains the dust cloud. Then we apply it to the pyramidal transform to enhance the image, we then apply the prominent direction estimation method described above. We did the analysis on band 4 of each image, since the results for both bands 4 and 5 were very similar.

1 – Apr 15th 2003

We first crop the region of the image that contains the dust cloud. We then apply the cropped image into the pyramidal filter to enhance the image; the result we got for this event after amplifying the high frequencies by 5 is shown in Fig 3.9

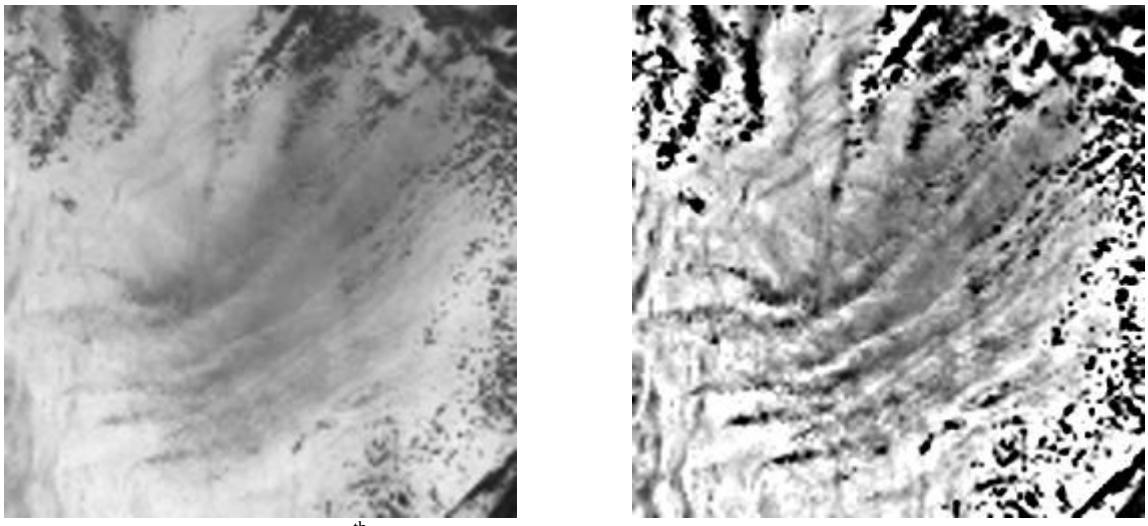

Fig 3.9: original image for Apr 15th 2003 (Left), the enhanced version of the image using the pyramidal filter

We then apply the enhanced image to the block processing to find the prominent direction. The result of this step is shown in Fig. 3.10

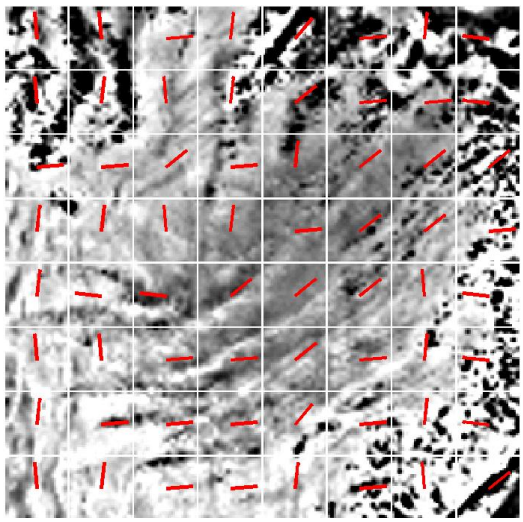

Fig 3.10: the red lines indicate the prominent direction of each block.

For clarity, we will provide the dominant angle of each block on Table 3.1.

Table: 3.1: the angle values for the red arrows of the Apr 15th event.

95	95	5	84	50	5	84	174
95	84	95	84	39	5	5	174
5	5	39	5	84	39	39	39
84	84	95	84	5	39	39	5
84	174	174	39	39	39	95	174
95	95	5	5	39	5	84	174
84	5	5	5	50	5	84	174
95	84	5	5	84	5	95	39

A shaded region is considered to be one entity; the blue one represents the direction of the dust cloud in the right half of the image, while the yellow region shows the direction in the left half of the image. Each number in the table represents the center of the angle range that is declared to be the prominent direction; let us take the angle 39° for example, it represents the band (39° ± 5°) which is the band (34° – 45°). The grouping of blocks happens only if their corresponding sub-bands are adjacent, like the case of 174° and 5°, or 39° and 50°. Also, we focus on the results that are within the dust cloud region.

2 – Dec 15th 2003

We applied the same analysis above to this event, after cropping the image and applying to the pyramidal filter, the results we got are shown in Fig 3.11

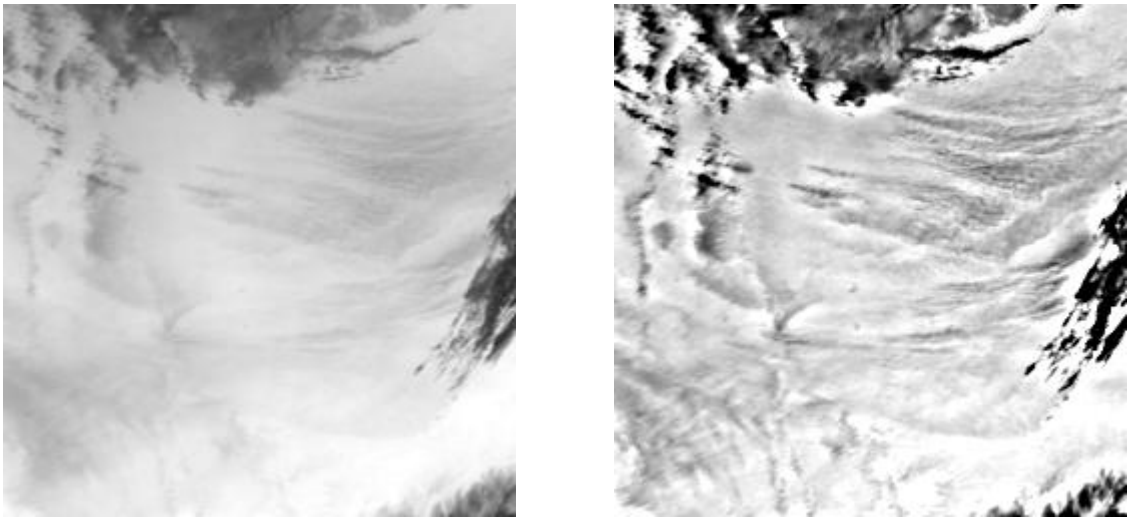

Fig 3.11: original image for Dec 15th 2003 (Left), the enhanced version of the image using the pyramidal filter

The results obtained from the prominent direction estimation are shown in Fig 3.12

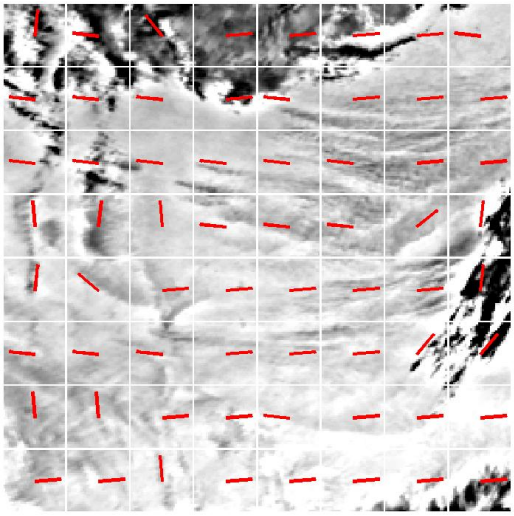

Fig 3.12: the prominent direction of each block

The angles of these red lines are shown in table 3.2.

Table 3.2: the angle values for the red arrows of the Dec 15th event.

84	174	129	5	5	5	5	174
174	174	174	5	174	5	5	5
174	174	174	174	174	174	5	5
95	84	95	174	174	174	39	84
84	140	5	5	5	5	5	84
174	174	174	5	5	5	50	50
95	95	5	5	174	5	5	5
5	5	95	5	5	5	5	5

Similarly, the grouping here happened between the angle 5° (sub-band 0° – 11°) and 174° (sub-band 169° – 180°) since these two sub-bands were close to horizontal, we combined both bands. Again we focused only on the dust cloud region.

3 – Dec 26th 2003

The input is shown on the left side of Figure 3.13, and the enhanced image is shown on the right.

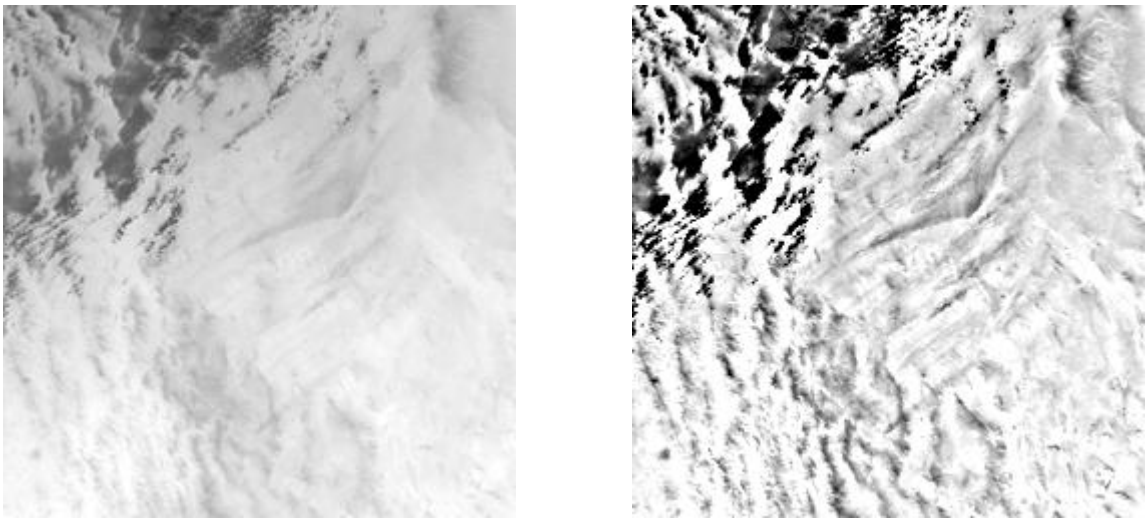

Fig. 3.13: original image for Dec 26th 2003 (Left), the enhanced version of the image using the pyramidal filter.

The dominant direction of each block is shown in Figure 3.14

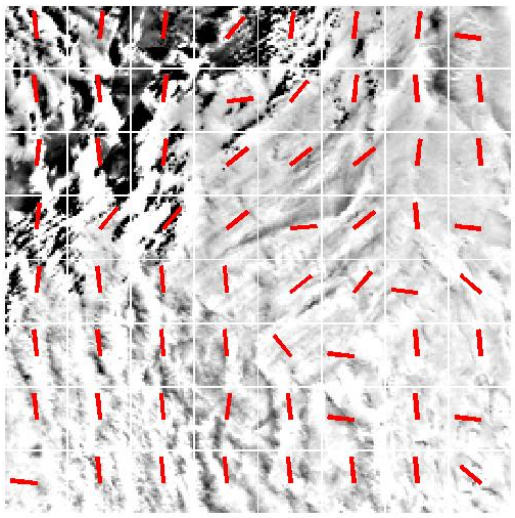

Fig 3.14: the prominent direction of each block for Dec 26th event.

The angles associated with the red arrows are shown in table 3.3, with the corresponding grouping of blocks.

Table: 3.3: the angle values for the red arrows of the Dec 26th event.

95	84	84	50	84	84	84	174
95	95	84	5	50	84	95	95
84	95	84	39	39	39	84	95
84	50	50	39	5	39	95	174
84	95	95	95	39	50	174	140
95	95	95	95	129	174	95	95
95	95	95	84	95	174	95	174
174	95	95	95	95	95	95	140

4 – Mar 04th 2003

The input is shown on the left side of Figure 3.15, and the enhanced image is shown on the right.

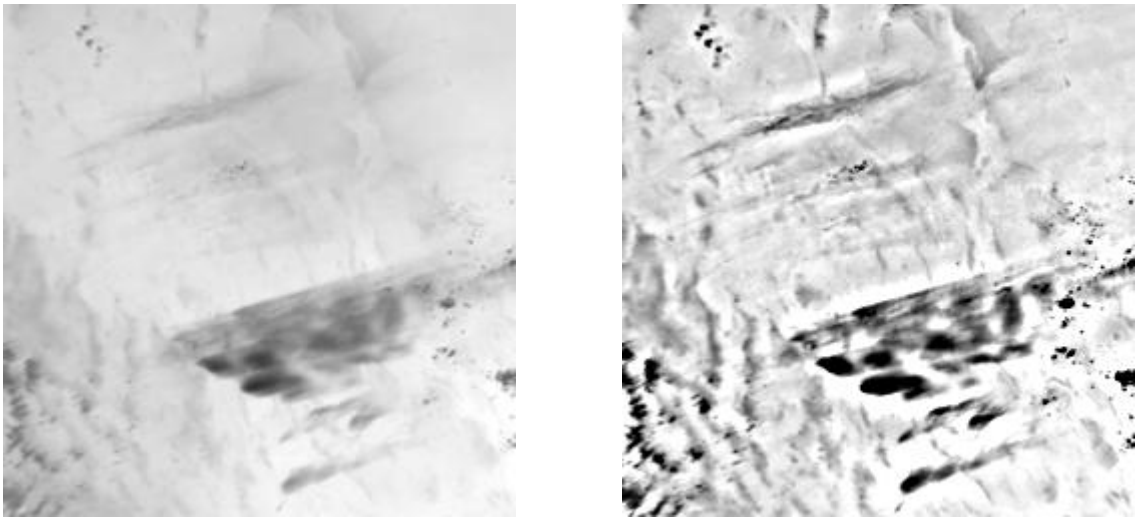

Fig. 3.15: original image for Mar 04th 2003 (Left), the enhanced version of the image using the pyramidal filter

Fig. 3.16 will show the results of the prominent direction estimation for each block, and table 3.4 shows corresponding angles of the red lines.

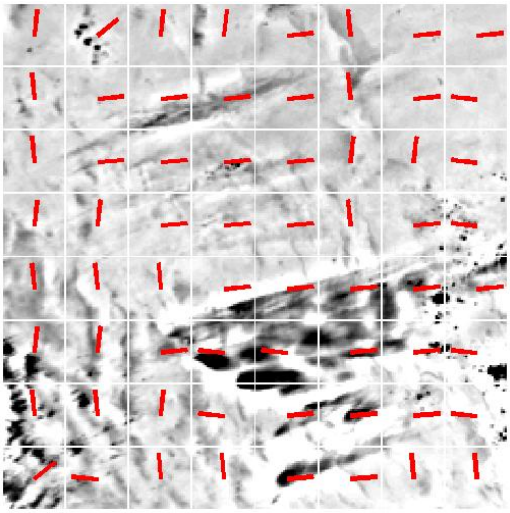

Fig 3.17: the prominent direction of each block for Dec 26th event

Table: 3.4: the angle values for the red arrows of the Mar 04th event.

84	39	84	84	5	95	5	5
95	5	5	5	5	95	5	174
95	5	5	5	5	84	84	174
84	84	5	5	5	95	5	174
95	95	95	5	5	5	5	5
84	84	5	174	174	5	5	174
95	95	84	174	5	5	5	174
39	174	95	95	5	5	95	95

CHAPTER 4

CONCLUSIONS AND FUTURE WORK

In the first part of the second chapter, we introduced a new method to locate dust clouds in NOAA-AVHRR satellite images; the method consists of a new approach to detect dust clouds using image segmentation based on the region growing algorithm, the results of this method were promising as most of the dust events were detected using this method. However, the need for band math analysis is still an essential step that our algorithms need as a starting point. Further studies and analysis of other possible spectral processing is highly recommended. One other thing is the threshold value that is used to find the seed points, the selection of this value was based on the user, further studies that involve the image histogram might help to automate the process of finding the threshold value.

In the second part of chapter 2, we focused our research on locating the dust sources in the satellite images. Starting with the dust cloud region already detected, the method involved the use of the Harris corner detection algorithm, the results were promising, however, due to the complex shape of dust region, the corner detector detects too many potential sources that cannot be assumed to be dust sources. To overcome this issue, a polygonal approximation has been applied to the perimeter of the dust cloud region, the results were improved for some events, not all, so there is a need for other methods to simplify the image contour without losing information, the use of the Rosenfeld-Johnson corner detector may make contours of the image look smoother. Also further work can be done to develop a new algorithm that detects corners based more precisely on their angle. This can be a good way to have more quantitative analysis regarding the corner detection.

Regarding the work in chapter 3, the results obtained can be considered to be a stepping stone to finding the exact direction of the dust storm at every location in the form of a vector field. Future work may involve using more levels in the directional filtering, in this research, the maximum number of levels used is 4, which means that we were limited to 16 directions; further research can be done to make the number of levels higher and data dependent adjusted to the uniformity of the direction within the image block. Future work may also involve the use of the full Contourlet transform to do the image enhancement together with directional filtering and prominent direction estimation.

REFERENCES

[1] David A. Landgrebe, [Signal Theory Methods in Multispectral Remote Sensing], Wiley-Interscience Publishers, 2003.

[2] Nahid Khazenie, Thomas F. Lee, "Identification of aerosol features such as smoke and dust, in NOAA-AVHRR data using spatial textures", Proceedings of IEEE International Geoscience and Remote Sensing Symposium IGARSS92, Houston Texas, May 1992.

[3] Hesham El-Askary, Menas Kafatos, Xue Liu, Tarek El-Ghazawi, "Introducing new approaches for dust storms detection using remote sensing technology," Proceedings of IEEE International Geoscience and Remote Sensing Symposium IGARSS03, Toulouse France, July 2003.

[4] Rivera-Rivera, N. I., [Detection and characterization of dust source areas in the Chihuahuan desert, Southwestern North America], Master's Thesis, Environmental Science and Engineering, University of Texas at El Paso (December 2006).

[5] Ackerman, S. A., "Remote sensing aerosols using satellite infrared observations", Journal of Geophysical Research 102, 17069-17079 (1997).

[6] Gonzalez, R. C. and Woods, R. E. [Digital Image Processing], 3^{rd} *ed.*, Prentice Hall, Upper Saddle River, NJ, 2008.

[7] Harris C. and Stephen M. "A combined corner and edge detection" In Matthews M. M., editor proceedings of the 4th ALVEY vision conference, pages 147 – 151, University of Manchester England, 1988.

[8] P. Rivas-Perea and J. G. Rosiles, "A Probabilistic Model for Stratospheric Soil-Independent Dust Aerosol Detection," in *Digital Image Processing and Analysis,* OSA Technical Digest (CD) (Optical Society of America, 2010), paper DMD4.

[9] S. Janugani, V. Jayaram, S. D. Cabrera, J. G. Rosiles, T. E. Gill and N. Rivera Rivera, "Directional analysis and filtering for dust storm detection in NOAA-AVHRR imagery", Proc. SPIE 7334, 73341G (2009).

[10] Mario I. Chacon-Murguía, Yearim Quezada-Holguín, Pablo Rivas-Perea and Sergio Cabrera Lecture Notes in Computer Science, 2011, Volume 6718, Pattern Recognition, Pages 305-313.

[11] Rivera-Rivera, N.R., Gill, T.E., Bleiweiss, M.P., and Hand, J.L., 2010. "Source characteristics of hazardous Chihuahuan Desert dust outbreaks". Atmospheric Environment 44: 2457- 2468.

[12] Sonka, M., Hlavac, V. Boyle, R.: [Image Processing, Analysis, and Machine Vision] Chapman and Hall Publishers, London – New York, 555 p., 1993.

[13] Cunha, A. L., Zhou, J., Do, M. N., "The nonsubsampled contourlet transform: Theory, design, and applications," IEEE Transactions on Image Processing, vol. 15, no. 10, pp. 3089-3101 (2006).

[14] Grant V. Welland, [Beyond Wavelets], Academic Press, 2003.

[15] M. N. Do and M. Vetterli, Framing pyramids, *IEEE Transactions on Signal Processing*, vol. 51, pp. 2329-2342, Sep. 2003.

[16] Bamberger, R. H., Smith,M. J. T., "A filter bank for the directional decomposition of images: Theory and design," IEEE Transactions on Signal Processing 40, no. 4, pp. 882-893 (1992).

[17] Zhou, J., da Cunha, A. L., Do, M. N., "Nonsubsampled contourlet transform: construction and application in enhancement," IEEE International Conference on Image Processing (2005).

[18] Scott E. Umbaugh, [Computer Imaging: Digital Image Analysis and Processing], CRC Press, 2005, ISBN 0-8493-2919-1

[18] *http://www.crisp.nus.edu.sg/~research/tutorial/intro.htm*

[19] *http://www.gsd.harvard.edu/pbcote/courses/gsd6322/remote_sensing/*

CURRICULUM VITAE

Mohammed Alkhatib was born on May 31, 1985 in Irbid, Jordan. He finished his bachelor degree in Telecommunications engineering on June, 2008 from the Hijjawi faculty for science and engineering, Yarmouk University, Irbid, Jordan.

In spring 2009, he entered the University of Texas at El Paso to pursue his Masters in Electrical Engineering. His areas of specialization include Digital Signal and Image Processing. He began his research work under the guidance of Dr. Sergio Cabrera. During his Masters Degree, he got his acceptance to pursue his PhD in same school; currently he is working as a teaching assistant in Electrical and Computer Engineering Dept.